

Manuscript structure: To avoid fragmentation and for ease of readability, tables S1 and S2 as well as Figures S3 to S9 should be moved to the main part of the paper. They are key parts of the Results and Discussion sections and in many cases referred to repeatedly in the text. Since Table S3 only adds one additional column with new values compared with Table 2, it should be merged with Table 2.

R: Thanks for the suggestion. We agree that Table S3 should be merged with Table 2. However, for the simplicity and readability of the manuscript, we cannot agree with including Tables S1 and S2 as well as Figures S3 to S9 in the main manuscript. For example, Tables S1 and S2 have been previously published (Harris et al., 2017 for Table S1; Sowers et al., 2002, Röckmann et al., 2003... for Table S2) and have been clearly referenced in our manuscript. For Figures S3 to S9, the contained information was mostly supportive or overlapping with the main manuscript. Therefore, we would rather keep them in the supporting information.

Data availability: Please upload all data used for the study to a publicly accessible archive and provide a Digital Object Identifier (DOI). It is not sufficient to have them available on request from the lead author. For details, please refer to https://www.atmospheric-chemistry-andphysics.net/about/data_policy.html

R: OK. This is done in the R2.

Mixing calculation: There is an error in your "Estimates of the combined effects from STE and soil emissions on $\delta^{15}\text{N}^{\text{SP}}$ ". The effect on δ due to mixing with stratospheric air is about three times larger than the 5 ‰ value you used. In contrast, the effect due to soil emission is too big and should be about three times smaller. However, overall, the combined effect is too small to be measured.

I think this is an important calculation and you should move it from the supplement to the main text (after correcting it as explained in the following).

Mixing with stratospheric air: The effect on tropospheric air can be approximated using the apparent isotopic fractionation ε_{app} (Kaiser et al. 2006). You can readily derive this from the slope of the Rayleigh fractionation equation at $y = y_{\text{T}}$ (where y_{T} is the N_2O mole fraction at the point the of mixing between troposphere and stratosphere):

$$\delta = (1 + \delta_0) f^{\epsilon_{\text{app}}} - 1 \quad \text{with } f = \frac{y}{y_T}$$

$$\frac{d\delta}{df} = (1 + \delta_0) \epsilon_{\text{app}} f^{\epsilon_{\text{app}} - 1}$$

$$y_T \frac{d\delta}{dy} = (1 + \delta_0) \epsilon_{\text{app}} \left(\frac{y}{y_T} \right)^{\epsilon_{\text{app}} - 1}$$

This gives

$$\lim_{y \rightarrow y_T} \frac{d\delta}{dy} = \frac{(1 + \delta_0) \epsilon_{\text{app}}}{y_T}$$

The derived slope is in agreement with the compact relationship between δ and N₂O mole fraction plotted in Fig. 5 of Kaiser et al. (2006). For the "site-preference" $\delta^{15}\text{N}^{\text{SP}}$, ϵ_{app} needs to be replaced with the difference between the

¹⁵N/¹⁴N isotope fractionations at the central and terminal N atoms, ${}^2\epsilon_{\text{app}} - {}^1\epsilon_{\text{app}}$ (or ${}^\alpha\epsilon_{\text{app}} - {}^\beta\epsilon_{\text{app}}$).

For the lower stratosphere, $\epsilon_{\text{app}} (\delta^{15}\text{N}^{\text{SP}}) \approx -15 \text{ ‰}$ (Kaiser et al. 2006), i.e. about three times larger than your value of 5 ‰.

Effect of soil emissions: I am not sure what you mean by the sentence "The isotopic effect of soil emission (−30‰), which is mainly attributed to the switch from nitrification to denitrification, is taken from Sutka et al. (2006)." It sounds as if you have taken the difference between the $\delta^{15}\text{N}^{\text{SP}}$ values of denitrification (0 ‰?) and nitrification (+30 ‰?). However, the relevant quantity here is the difference between the $\delta^{15}\text{N}^{\text{SP}}$ values of soil emissions (+7.3 ‰; Table 3) and tropospheric air (+18 ‰; Fig. 2), i.e. −10.7 ‰, i.e. three times smaller than your estimate. *Overall effect:* Since your estimate N₂O mole fraction enhancement due to emissions (0.15-0.2 nmol mol^{−1}) is about twice the N₂O mole fraction depletion due to mixing with stratospheric air (−0.35-0.4 nmol mol^{−1}), the net effect is $[(-0.4 \text{ nmol mol}^{-1})(-15 \text{ ‰}) + (0.2 \text{ nmol mol}^{-1})(-10.7 \text{ ‰})] / (330 \text{ nmol mol}^{-1}) = 0.01 \text{ ‰}$. In other words, the effect due to STE dominates, but is too small to be measured.

R: We really appreciate the editor's explanation and suggestion. Now we have corrected our estimates of the combined effects from STE and soil emissions on $\delta^{15}\text{N}^{\text{SP}}$ and have implemented details of mixing calculation to M&M. Accordingly, we have rewritten our discussion of seasonal patterns of N₂O isotopic signatures in Section 4.2-R2.

Other corrections:

Röckmann, not Rockmann

R: OK, corrected.

Units and chemical symbols should not be mixed. Please express mass fluxes as "Tg a⁻¹ N equivalents" or " Tg a⁻¹ N" with a short explanation what this means upon first usage.

ACP requires adhering to the International System of Units (SI) and the Recommendations in the IUPAC Green Book (https://www.atmospheric-chemistry-andphysics.net/for_authors/manuscript_preparation.html)

R: OK, we have corrected it as requested.

Please use a suitable (single-letter) quantity symbol for the troposphere-stratosphere air exchange flux (e.g. F_{TS} or F_{ex}).

R: OK, we use F_{ex} now.

l. 174 & 175: Please use SI units for mole fractions, i.e. nmol mol⁻¹ (not ppb).

l. 301: Ditto, but "pmol mol⁻¹".

R: OK, done.

l. 240: What is the remaining 1 %? Even with rounding errors, the values of 78 % and 21 % cannot add up to 100 %.

R: This is a mistake. We have changed it in R2.

l. 673: Please replace "species" with "deltas".

R: This is corrected in R2.

Table S2: The uncertainty range for the stratosphere-troposphere exchange rate is too wide. In particular, it cannot be negative.

R: Sorry for the mistake. It is "(5.37±1.26) x 10¹⁷" instead and we have corrected this in Table S2.

Tables 2 & S3: You should add the estimates of Röckmann et al. 2003 to the table since you cite our study on various occasions. You may need to make an assumption on the modern tropospheric values on international scales (e.g. use your measurements). An alternative idea would be to express the source signatures of each study relative to the modern value, to avoid biases due to different isotope calibration scales. The source vs. troposphere δ differences are more robust than the absolute values.

R: OK. We have now included the estimates from Röckmann et al. (2003) for comparison. These δ values for anthropogenic sources were calculated using the modern tropospheric values from this study. Although expressing the source signatures relative to modern values may help to reduce the biases from different calibration scales, it is rather difficult to justify whether overall mean δ values observed from the modern troposphere or values from the same years should be chosen for comparison, given that these studies from literature span over two decades. We will consider this approach in future study.

Tables 2 and S3: The internationally accepted abbreviation for "year" is "a" (from Latin annum). You actually use the symbol "a" elsewhere in the manuscript.

R: OK. Replaced.

Your responses to queries 19 and 20 of referee #2 are missing.

19. L 461: Comparing Figure 3(a) in Toyota et al. (2013) with Figure 1a here, it does not look “almost identical”, but perhaps comparable. The monthly mixing ratio of N₂O at Jungfraujoch is at maximum in June while in April at Hateruma Island, Japan.

R: Agree. We have changed the description to “comparable”.

20. L 464: What are the underlying mechanisms?

R: We actually mean “the explanation of temporal patterns of N₂O isotopic signatures can be complicated by variable N₂O sources”. This is now revised in section 4.2.

List of all relevant changes (referred to Line numbers in R2):

Line 90: “Tian et al., 2018” to “**Tian et al., 2019**”.

Line 174-175: “ppb” changed to “**nmol mol⁻¹**”.

Line 240: “78% N₂ and 21% O₂” changed to “**78% N₂ and 21% O₂**”.

Line 301: “criteria” to “**criterion**”.

Line 302: “ppt” to “**pmol mol⁻¹**”.

Line 323-324: “*T*Sex” to “***F*ex**”.

Line 343-364: Add section 2.8 “**Evaluation of the combined effects from STE and soil emission on $\delta^{15}\text{N}^{\text{SP}}$** ” for the mixing calculation.

Line 365: “2.8” to “**2.9**”.

Line 425: “Tg N₂O-N a⁻¹” to “**Tg N₂O-N a⁻¹ equivalents**”.

Line 497: “almost identical to” to “**which is comparable with**”.

Line 499-500: “complicating the underlying mechanisms for the observed pattern” to “**complicating the explanations for the observed temporal pattern**”.

Line 510: “observe” to “**observed**”.

Line 514: “Figure 5a&b” to “**Figure 6a&6b**”.

Line 521-533: Rewrite the discussion of “**minimum of $\delta^{15}\text{N}^{\text{SP}}$ in late summer and the results from mixing calculation**”.

Line 642: “Table S3” to “**Table 2**”.

Line 653: Add “**Röckmann et al., 2003**”.

Line 721: “species” to “**deltas**”.

Line 729-730: Add data source “**Data for this study have been deposited in a general data repository (<https://figshare.com/s/077562ab408dd1bd0880>; doi:10.6084/m9.figshare.12032760.v1, 2020)**”.

Line 845-847: Add reference “**Kaiser et al., 2006**”.

Table 2: Merged with Table S3 and also included the estimates from “**Röckmann et al., 2003**” for comparison.

1 **The isotopic composition of atmospheric nitrous oxide**
2 **observed at the high-altitude research station Jungfrauoch,**
3 **Switzerland**

4 Longfei Yu^{1*}, Eliza Harris^{1†}, Stephan Henne¹, Sarah Eggleston¹, Martin Steinbacher¹, Lukas
5 Emmenegger¹, Christoph Zellweger¹ and Joachim Mohn¹

6 ¹Laboratory for Air Pollution & Environmental Technology, Empa, Swiss Federal Laboratories
7 for Materials Science and Technology, Ueberlandstr. 129, CH-8600 Duebendorf, Switzerland.

8 [†]Current address: Institute of Ecology, University of Innsbruck, Sternwartestrasse 15, A-6020
9 Innsbruck, Austria

10 * Correspondence: L. Yu (longfei.yu@empa.ch)

11

12 **Abstract**

13 Atmospheric nitrous oxide (N₂O) levels have been continuously growing since preindustrial times.
14 Mitigation requires information about sources and sinks on the regional and global scales. Isotopic
15 composition of N₂O in the atmosphere could contribute valuable constraints. However, isotopic
16 records of N₂O in the unpolluted atmosphere remain too scarce for large-scale N₂O models. Here,
17 we report the results of discrete air samples collected weekly to bi-weekly over a five-year period
18 at the high-altitude research station Jungfraujoch, located in central Switzerland. High-precision
19 N₂O isotopic measurements were made using a recently developed preconcentration-laser
20 spectroscopy technique. The measurements of discrete samples were accompanied by *in situ*
21 continuous measurements of N₂O mixing ratios. Our results indicate a pronounced seasonal pattern
22 with minimum N₂O mixing ratios in late summer, associated with a maximum in $\delta^{15}\text{N}^{\text{bulk}}$ and a
23 minimum in intramolecular ¹⁵N site preference ($\delta^{15}\text{N}^{\text{SP}}$). This pattern is most likely due to
24 stratosphere-troposphere exchange (STE), which delivers N₂O-depleted but ¹⁵N-enriched air from
25 the stratosphere into the troposphere. Variability in $\delta^{15}\text{N}^{\text{SP}}$ induced by changes in STE may be
26 masked by biogeochemical N₂O production processes in late summer, which are possibly
27 dominated by a low- $\delta^{15}\text{N}^{\text{SP}}$ pathway of N₂O production (denitrification), providing an explanation
28 for the observed seasonality of $\delta^{15}\text{N}^{\text{SP}}$. Footprint analyses and atmospheric transport simulations
29 of N₂O for Jungfraujoch suggest that regional emissions from the planetary boundary layer
30 contribute to seasonal variations of atmospheric N₂O isotopic composition at Jungfraujoch, albeit
31 more clearly for $\delta^{15}\text{N}^{\text{SP}}$ and $\delta^{18}\text{O}$ than for $\delta^{15}\text{N}^{\text{bulk}}$. With the time-series of five years, we obtained
32 a significant interannual trend for $\delta^{15}\text{N}^{\text{bulk}}$ after deseasonalization ($-0.052\pm 0.012\text{‰ a}^{-1}$), indicating
33 that the atmospheric N₂O increase is due to isotopically depleted N₂O sources. We estimated the
34 average isotopic signature of anthropogenic N₂O sources with a two-box model to be $-8.6\pm 0.6\text{‰}$

35 for $\delta^{15}\text{N}^{\text{bulk}}$, $34.8\pm 3\text{‰}$ for $\delta^{18}\text{O}$ and $10.7\pm 4\text{‰}$ for $\delta^{15}\text{N}^{\text{SP}}$. Our study demonstrates that seasonal
36 variation of N_2O isotopic composition in the background atmosphere is important when
37 determining interannual trends. More frequent, high-precision and inter-laboratory compatible
38 measurements of atmospheric N_2O isotopocules, especially for $\delta^{15}\text{N}^{\text{SP}}$, are needed to better
39 constrain anthropogenic N_2O sources, and thus the contribution of biogeochemical processes to
40 N_2O growth on the global scale.

41 **1 Introduction**

42 Nitrous oxide (N₂O) is a potent greenhouse gas (Fowler et al., 2015) and a strong stratospheric
43 ozone-depleting substance (Ravishankara et al., 2009). For several decades, near-surface
44 atmospheric N₂O mixing ratios have been continuously measured at a series of remote sites, within
45 the networks of the Global Atmosphere Watch Programme (JMA and WMO, 2018), the Advanced
46 Global Atmospheric Gases Experiment (AGAGE) (Prinn et al., 2018), and the National Oceanic
47 and Atmospheric Administration (NOAA) Earth System Research Laboratory (ESRL) Global
48 Monitoring Division (GMD) (Nevison et al., 2011). These measurements have shown a significant
49 increase in atmospheric N₂O mixing ratio, at a current growth rate of about 0.93 nmol mol⁻¹ a⁻¹
50 (WMO, 2018). On the global scale, given excessive nitrogen (N) fertilizer application, agriculture
51 is known to be the largest and most important anthropogenic source of N₂O (Reay et al., 2012;
52 Tian et al., ~~2018~~2019). However, long-term observations of N₂O in the unpolluted atmosphere
53 have shown seasonal and interannual variabilities as well as interhemispheric differences in N₂O
54 mixing ratios (Nevison et al., 2011; Thompson et al., 2014a, 2014b), which cannot yet be resolved
55 by atmospheric transport models and existing emission inventories. Moreover, regional
56 contributions of N₂O emissions and the strengths of individual N₂O production pathways remain
57 difficult to quantify.

58 Isotopic signatures of atmospheric N₂O can provide important constraints on N₂O sources (Denk
59 et al., 2017) and trends (Kim and Craig, 1993). The ratios of ¹⁵N/¹⁴N and ¹⁸O/¹⁶O in N₂O are often
60 reported in δ notation as $\delta(^{15}\text{N}/^{14}\text{N})$ and $\delta(^{18}\text{O}/^{16}\text{O})$, abbreviated as $\delta^{15}\text{N}^{\text{bulk}}$ (average for ¹⁴N¹⁵N¹⁶O
61 and ¹⁵N¹⁴N¹⁶O) and $\delta^{18}\text{O}$, respectively. A large fraction of N₂O emitted to the atmosphere
62 originates from soil bacterial processes, which usually emit N₂O that is more enriched in light (¹⁴N,
63 ¹⁶O) isotopes than the tropospheric background (Pérez et al., 2001; Snider et al., 2015a; Toyoda et

64 al., 2017). By contrast, N₂O produced in the oceans (Bourbonnais et al., 2017; Fujii et al., 2013)
65 and emitted from fossil fuel combustion (Ogawa and Yoshida, 2005; Toyoda et al., 2008) has
66 higher $\delta^{15}\text{N}^{\text{bulk}}$ and $\delta^{18}\text{O}$ values which are comparable to the tropospheric background. A recent
67 study has summarized isotopic signatures of anthropogenic N₂O sources divided into the EDGAR
68 (Emissions Database for Global Atmospheric Research) emission categories (Janssens-Maenhout
69 et al., 2019), showing differences in isotopic signatures between agricultural ($\delta^{15}\text{N}^{\text{bulk}} = -17.8$ to -
70 1.0‰ and $\delta^{18}\text{O} = 23.9$ to 29‰) and industrial sources ($\delta^{15}\text{N}^{\text{bulk}} = -28.7$ to 5.5‰ and $\delta^{18}\text{O} = 28.6$
71 to 40.3‰) (Harris et al., 2017). These empirical ranges, together with isotopic mixing models,
72 provide a valuable approach to interpret variability in atmospheric N₂O mixing ratios.

73 A number of studies have analyzed temporal trends in N₂O isotopic composition in the modern
74 atmosphere (Kaiser et al., 2003; Park et al., 2012; Röckmann and Levin, 2005; Toyoda et al., 2013)
75 and in the past from firn and ice cores (Bernard et al., 2006; Ishijima et al., 2007; Prokopiou et al.,
76 2018; Röckmann et al., 2003; Sowers et al., 2002). These isotopic measurements have shown a
77 decrease in both $\delta^{15}\text{N}^{\text{bulk}}$ - and $\delta^{18}\text{O}$ -N₂O associated with an increasing trend in atmospheric N₂O
78 mixing ratios since preindustrial times, indicating that the recent increase of atmospheric N₂O may
79 be due to agricultural emissions (¹⁵N and ¹⁸O depleted). The reported trend since the 1960s seems
80 rather steady (-0.034 ± 0.005 ‰ a⁻¹ for $\delta^{15}\text{N}^{\text{bulk}}$ and -0.016 ± 0.006 a⁻¹ for $\delta^{18}\text{O}$) (Bernard et al.,
81 2006; Ishijima et al., 2007; Park et al., 2012; Prokopiou et al., 2017; Röckmann et al., 2003;
82 Röckmann and Levin, 2005). However, a more recent (1999-2010) study reported a smaller
83 decreasing trend in $\delta^{15}\text{N}^{\text{bulk}}$ and only an insignificant trend in $\delta^{18}\text{O}$ for the Northern Hemisphere
84 (Toyoda et al., 2013). Several hypotheses were proposed to explain the differences in the observed
85 trends: 1) the interhemispheric difference in N₂O emission sources results in inconsistent isotopic
86 signatures among different studies (Thompson et al., 2014b); 2) uncertainties in isotopic

87 measurements and variable sampling schemes (air type, sampling frequency and time) mask the
88 small secular trend of N₂O isotopic composition in the background atmosphere (Toyoda et al.,
89 2013); and/or 3) N₂O source isotopic signatures have changed in recent years, possibly due to
90 shifts in N fertilizer type and climatic forcing (Tian et al., 2018~~9~~⁹). Hence, further investigation into
91 the global N₂O source inventory and its evolution over time requires more frequent, precise
92 measurements of N₂O isotopocules in the unpolluted atmosphere, particularly in the Northern
93 Hemisphere.

94 Recently, site-specific composition of N₂O isotopomers (site preference: $\delta^{15}\text{N}^{\text{SP}}$), which denotes
95 the difference of ¹⁵N between the central (¹⁴N¹⁵N¹⁶O, α position) and terminal (¹⁵N¹⁴N¹⁶O, β
96 position) N atoms, has been applied to constrain sources contributing to atmospheric N₂O (Toyoda
97 et al., 2013; Yoshida and Toyoda, 2000). $\delta^{15}\text{N}^{\text{SP}}$ of N₂O is particularly effective for distinguishing
98 between the major N₂O production processes, i.e. nitrification and denitrification, generally
99 referred to as aerobic and anaerobic N₂O production, with high and low $\delta^{15}\text{N}^{\text{SP}}$, respectively (Sutka
100 et al., 2006). However, despite the advantages of $\delta^{15}\text{N}^{\text{SP}}$ measurements, existing long-term studies
101 have not yet been able to reach a definitive understanding of the $\delta^{15}\text{N}^{\text{SP}}$ -N₂O trend, showing both
102 positive (Bernard et al., 2006; Park et al., 2012; Röckmann and Levin, 2005) and negative
103 tendencies (Röckmann et al., 2003) over the last four decades. This is probably due to an
104 insufficient analytical precision and poor inter-laboratory agreement, in particular as the
105 aforementioned studies are all based on isotope ratio mass spectrometry (IRMS). To retrieve site-
106 specific isotopic information by IRMS, the N₂O⁺ molecular ions and the NO⁺ fragment ions are
107 analyzed and raw data have to be corrected for rearrangements of central and terminal N and ¹⁷O
108 content (Toyoda et al., 2001). Inappropriate correction algorithms and the limited availability of

109 reference materials (Ostrom et al., 2018) further enlarge the analytical uncertainty (Mohn et al.,
110 2014).

111 Seasonal variability in atmospheric N₂O isotopic composition, which could affect the longer-term
112 trends, is still rarely reported in the literature (Park et al., 2012; Toyoda et al., 2013). Moreover,
113 studies of seasonality of N₂O isotopic composition are limited to the recent past since the air
114 samples derived from firn and ice cores suffer from coarse temporal resolution (< 2 samples per
115 year). Park et al. (2012) studied seasonality of atmospheric N₂O isotopic composition by analyzing
116 a set of archived air samples collected from Cape Grim (Australia) using a sophisticated
117 mathematical modeling approach. They found consistent seasonal patterns in $\delta^{15}\text{N}^{\text{bulk}}$, $\delta^{18}\text{O}$ and
118 $\delta^{15}\text{N}^{\text{SP}}$ of atmospheric N₂O, showing highest ¹⁵N/¹⁸O enrichment in June and lowest in December.
119 This pattern was negatively correlated with the seasonality of the N₂O mixing ratios (lowest in
120 April-May and highest in December), which is in agreement with a previous study by Nevison et
121 al. (2011). The negative correlation between isotopic composition and mixing ratios has been
122 explained by stratosphere-troposphere exchange (STE), which transports N₂O-depleted but
123 isotopically enriched stratospheric air (prevailing reduction process) into the lower atmosphere
124 (Yung and Miller, 1997). However, in a more recent study from Hateruma Island (Japan), Toyoda
125 et al. (2013) reported insignificant seasonal patterns in atmospheric N₂O isotopocules (smaller
126 variability than measurement precision), despite their finding of a somewhat similar seasonal
127 pattern in N₂O mixing ratio (minimum in July). Although there are interhemispheric differences
128 in N₂O sources and distinct sampling frequencies in the two studies discussed above (2-3 times
129 per year versus monthly), it is noteworthy that both studies observed significantly larger variability
130 in $\delta^{15}\text{N}^{\text{SP}}$ than in $\delta^{15}\text{N}^{\text{bulk}}$ and $\delta^{18}\text{O}$. Whether the fluctuations in $\delta^{15}\text{N}^{\text{SP}}$ are mainly caused by the

131 limited repeatability of the chosen analytical techniques or interplay of processes or mechanisms
132 regulating atmospheric N₂O remains to be tested (Park et al., 2012).

133 With inherent selectiveness, in particular for site-specific isotopic composition, laser spectroscopy
134 provides a new analytical approach for direct, precise measurements of all four N₂O isotopocules
135 (Harris et al., 2014; Mohn et al., 2012). The recent development of quantum cascade laser
136 absorption spectroscopy (QCLAS) coupled with an automated preconcentration unit has been
137 applied to measure N₂O isotopocules in ambient air, with comparable precision for $\delta^{15}\text{N}^{\text{bulk}}$ and
138 $\delta^{18}\text{O}$ and superior precision for $\delta^{15}\text{N}^{\text{SP}}$ relative to IRMS systems (Harris et al., 2017; Mohn et al.,
139 2014). Here, we present results from the application of a preconcentration unit coupled to QCLAS
140 to measure atmospheric N₂O isotopocules in background air collected at the high altitude research
141 station Jungfraujoch, Switzerland. Between April 2014 and December 2018, we collected weekly
142 to bi-weekly air samples for N₂O isotopic analyses, in parallel with online measurement of N₂O
143 mixing ratios. To our knowledge, this work reports the first time-series of background atmospheric
144 N₂O isotopic composition using laser spectroscopy. With this unique dataset, we aim to 1)
145 constrain seasonal patterns of three N₂O isotopic signatures at the Jungfraujoch observatory; 2)
146 determine interannual trends in N₂O isotopocules, especially $\delta^{15}\text{N}^{\text{SP}}$; and 3) interpret the observed
147 patterns in N₂O mixing ratios using temporal trends in N₂O isotopic composition and reported
148 isotopic signatures of anthropogenic sources.

149 **2 Materials and Method**

150 **2.1 Site description**

151 The high altitude research station Jungfraujoch (3580 m above sea level), located on the northern
152 ridge of the Swiss Alps, is a well-established site for studying unpolluted atmosphere over Central
153 Europe (e.g. Buchmann et al., 2016). Although the station is located in the free troposphere most
154 of the time, it is occasionally affected by air recently lifted from the planetary boundary layer
155 (Herrmann et al., 2015; Zellweger et al., 2003). Henne et al. (2010) investigated the
156 representativeness of 35 European monitoring stations and categorized Jungfraujoch as “mostly
157 remote”. The Jungfraujoch station is part of several national and international networks, like the
158 meteorological SwissMetNet network operated by MeteoSwiss, the Swiss National Air Pollution
159 Monitoring Network (NABEL), the Global Atmospheric Watch Programme (GAW) of the World
160 Meteorological Organization (WMO) and the Integrated Carbon Observation Systems (ICOS)
161 Research Infrastructure. This results in an extended set of long-term and continuously available
162 parameters such as meteorological variables (Appenzeller et al., 2008), greenhouse gases (Schibig
163 et al., 2015; Sepúlveda et al., 2014; Yuan et al., 2018), CO₂ isotopic composition (Sturm et al.,
164 2013; Tuzson et al., 2011), ozone-depleting substances and their replacement products (Reimann
165 et al., 2008), atmospheric pollutants (Logan et al., 2012; Pandey Deolal et al., 2012; Zellweger et
166 al., 2009) and aerosol parameters (Bukowiecki et al., 2016).

167 **2.2 *In situ* measurements and discrete air sampling (flasks)**

168 *In situ* observations of N₂O mixing ratios commenced at Jungfraujoch in December 2004. Initially,
169 measurements were made with gas chromatography (GC) (Agilent 6890N, USA) followed by
170 electron capture detection (ECD). The time resolution of these measurements was 24 to 30 minutes.

171 In late 2014, we implemented a cavity-enhanced off-axis integrated cavity out-put spectroscopy
172 analyzer (OA-ICOS, Los Gatos Research Inc., Mountain View, CA, USA), which measures the
173 atmospheric N₂O mixing ratio continuously. Measurements of N₂O mixing ratios at Jungfraujoch
174 were calibrated with three standard gases (319, 327 and 342 ppb nmol mol⁻¹) and accompanied
175 with measurement of a working standard (331 nmol mol⁻¹ ppb) every 160 minutes to account for
176 instrumental drift. In addition, ~~daily~~-short- (two times every 40 hours) and long-term (every 40
177 hours) -target measurements were included to monitor the data quality to account for instrumental
178 drift long terms. Due to the superior measurement precision compared to the GC-ECD method
179 (Lebeque et al., 2016), the OA-ICOS record has become the primary time-series since January
180 2015. The GC-ECD observations continued until summer 2016 for comparison and quality control.

181 Additional parameters, recorded within the NABEL network and the ICOS infrastructure, were
182 included in the analysis below. These data were carbon monoxide (CO) (measured by cavity ring-
183 down spectroscopy; Model G2401, Picarro Inc., USA), the sum of oxidized nitrogen species (NO_y)
184 (measured by chemiluminescence detection after conversion of NO_y to NO on a heated gold
185 catalyst; CLD 89p, Eco Physics, Switzerland) and O₃ (measured by UV absorption; TEI 49i,
186 Thermo Scientific, USA). Details on measurement methods and calibration strategies can be found
187 in Zellweger et al. (2009) for CO, Pandey Deolal et al. (2012) for NO_y and Logan et al. (2012) for
188 O₃.

189 In conjunction with the online measurements, we deployed an automated sampling system (Fig.
190 S1) to collect pressurized air samples in aluminum cylinders from the same air inlet at the Sphinx
191 observatory in of the Junfraujoch station, for subsequent N₂O mixing ratio and isotopic analyses.
192 The sample collection was conducted weekly from April 2014 to February 2016. After a sampling
193 gap of five months due to a technical failure, we reinitiated a bi-weekly sampling, which continued

194 from August 2016 to December 2018. The sampling system, automated by a customized LabVIEW
195 program (National Instruments Corp., USA), consisted of a Nafion drier (PD-100T-48MSS, Perma
196 Pure LLC, USA), a membrane gas compressor (KNF Neuberger, USA; Type N286 series), a 16-
197 port selector valve (EMT2CSD16MWEPEH, VICI AG, Switzerland), and a rack to accommodate
198 nine 2-L aluminum flasks (Luxfer, Messer Schweiz AG, Switzerland). During sample filling, pre-
199 evacuated flasks were first purged with ambient air five times (1 hour), and then filled to 12000
200 hPa within 40 min, resulting in approximately 24 L (298 K and 1000 hPa) of air per flask for
201 isotopic analysis. Air sample filling generally took place between 2:00 and 3:00 pm local time at
202 each sampling day. Sample flasks were sent back to the laboratory at Empa for analyses every few
203 months. For this study, 142 air samples were collected in flasks and analyzed for N₂O isotopocules.

204 **2.3 Analyses of discrete air samples**

205 Discrete air samples were regularly analyzed in batches but note in chronological order to prevent
206 the imprint of analytical drifts on temporal trends of the samples. N₂O mole fractions were
207 analyzed by QCLAS (CW-QC-TILDAS-76-CS, Aerodyne Research Inc., USA) against NOAA
208 standards on the WMO-X2006A calibration scale (Hall et al., 2007), at a precision around 0.1
209 nmol mol⁻¹ (determined with the average of 1-min data).

210 The four most abundant N₂O isotopocules (¹⁴N¹⁴N¹⁶O, 99.03%; ¹⁴N¹⁵N¹⁶O, 0.36%; ¹⁵N¹⁴N¹⁶O,
211 0.36%; ¹⁴N¹⁴N¹⁸O, 0.20%) were analyzed using a customized QCLAS system (Aerodyne Research,
212 Inc., USA) (Heil et al., 2014) coupled with an automated preconcentration device (Mohn et al.,
213 2010). Before entering the pre-concentration unit, sample air is passed through a Sofnocat 423 trap
214 (Molecular Products Limited, GB) to remove CO, and subsequently through an Ascarite trap
215 (Ascarite: 6 g, 10–35 mesh, Sigma Aldrich, Switzerland, bracketed by Mg(ClO₄)₂, 2 × 1.5 g, Alfa
216 Aesar, Germany) to remove CO₂ and water. Approximately 5.5 L of air with a flow of 250 ml min⁻¹

217 ¹ (at 295 K and 3500 hPa) is then passed through a HayeSep D trap cooled to -145 °C to collect
218 N₂O (Mohn et al., 2010). For N₂O release to the multipath cell of the QCLAS, the HayeSep D trap
219 is quickly heated to 10 °C and flushed with high-purity synthetic air (20.5% of O₂ in N₂) carrier
220 gas at a flow rate of 25 ml min⁻¹ (at 295 K and 3500 hPa). A final cell pressure around 16 hPa is
221 achieved, which results in an N₂O mixing ratio of about 45 μmol mol⁻¹. More instrumental details
222 can be found in previous studies (Harris et al., 2017; Mohn et al., 2010, 2012). Sample tanks were
223 each analyzed twice to yield duplicates for N₂O isotopic results, which left sufficient air for amount
224 fraction analysis as described in the previous paragraph.

225 **2.4 Data analyses**

226 We used 10-minute averages of the continuous *in situ* measurements from the Jungfraujoch station
227 across this study. For a point-to-point comparison of continuous and discrete measurements of
228 N₂O mixing ratio, we aggregated 10-minute averages of *in situ* data for the same period when the
229 discrete sample was filled into the cylinder (40 min).

230 In this study, we report abundances of N₂O isotopocules using δ notation (‰) as below:

$$231 \quad \delta X = \frac{(R_{sample} - R_{standard})}{R_{standard}} \quad (1)$$

232 where X refers to ¹⁵N^α (¹⁴N¹⁵N¹⁶O), ¹⁵N^β (¹⁵N¹⁴N¹⁶O) and ¹⁸O (¹⁴N¹⁴N¹⁸O); R refers to the ratio
233 between the amount fractions of the rare isotopocules as mentioned above and the amount fraction
234 of ¹⁴N¹⁴N¹⁶O; isotope standards refer to atmospheric N₂ for ¹⁵N and Vienna Standard Mean Ocean
235 Water (VSMOW) for ¹⁸O.

236 Hence, the total ¹⁵N content of N₂O and site-specific composition of N₂O isotopomers could be
237 further illustrated as δ¹⁵N^{bulk} and δ¹⁵N^{SP}, respectively, according to the equations below:

238
$$\delta^{15}N^{bulk} = (\delta^{15}N^{\alpha} + \delta^{15}N^{\beta})/2 \quad (2)$$

239
$$\delta^{15}N^{SP} = \delta^{15}N^{\alpha} - \delta^{15}N^{\beta} \quad (3)$$

240 Two standards (CG1 and, CG2; in 79.58% N₂ and 20.51% O₂) with distinct isotopic signatures
241 ($\delta^{15}N^{\alpha} = 16.29 \pm 0.07\text{‰}$ (CG1) and $-51.09 \pm 0.07\text{‰}$ (CG2); $\delta^{15}N^{\beta} = -2.59 \pm 0.06\text{‰}$ and $-48.12 \pm$
242 0.04‰ ; $\delta^{18}O = 39.37 \pm 0.04\text{‰}$ and $30.81 \pm 0.03\text{‰}$) were used for calibrating isotopic composition.
243 The calibration gases CG1 and CG2 were calibrated on the Tokyo Institute of Technology (TIT)
244 scale, based on cross-calibration with primary standards assigned by TIT (Mohn et al., 2012, 2014).
245 In addition, CG1 was measured repeatedly between samples and target gases to account for
246 instrumental drift. Both CG1 and CG2 have N₂O mixing ratios of 45 $\mu\text{mol mol}^{-1}$, similar to the
247 N₂O amount fraction of the samples after preconcentration. However, to correct for possible
248 instrumental dependence on N₂O mixing ratio, CG1 was diluted to N₂O mole fractions of 35-40
249 $\mu\text{mol mol}^{-1}$ within each measurement batch. In general, duplicated isotopic measurements of flask
250 samples yielded values of repeatability of 0.10-0.20‰ for $\delta^{15}N^{bulk}$ and $\delta^{18}O$, and 0.15-0.25‰ for
251 $\delta^{15}N^{SP}$.

252 At the beginning of the project, a batch of three cylinders (50 L water volume, Luxfer, Italy) were
253 filled with pressurized ambient air in Dübendorf with an oil-free, three stage compressor (SA-3,
254 Rix Industries, USA) and used as long-term target gases. The pressurized ambient air target gas
255 was analyzed with identical treatment as Jungfraujoch air samples during every analysis batch, to
256 monitor long-term analytical drift. Standard deviations for repeated target gas measurements
257 throughout the period of Jungfraujoch sample measurements, were 0.13‰ for $\delta^{15}N^{bulk}$, 0.21‰ for
258 $\delta^{15}N^{SP}$, and 0.11‰ for $\delta^{18}O$ (Fig. S2).

259 **2.5 Surface air footprint analysis and simulated regional N₂O enhancement**

260 We analyzed the air mass origin at Jungfraujoch by applying the Lagrangian particle dispersion
261 model (LPDM) FLEX-PART in the backward mode (Stohl et al., 2005). The model was driven by
262 meteorological fields taken from the ECMWF-IFS operational analysis cycle, extracted at a
263 resolution of $1^\circ \times 1^\circ$, 90/137 levels globally, and at higher horizontal resolution of $0.2^\circ \times 0.2^\circ$ for
264 central Europe. We released 50000 virtual air parcels every 3 hours at 3000 m a.s.l. from
265 Jungfraujoch to perform backward dispersion simulations over 10 days, which allowed us to
266 calculate surface source sensitivities (concentration footprints). A release height of 3000 m a.s.l.
267 was previously determined to be an optimum for simulating concentration footprints at
268 Jungfraujoch, given the stated horizontal resolution which results in a considerable smoothing of
269 the complex, alpine orography (Keller et al., 2012). The 3-hourly surface footprints for the whole
270 observation period were used to categorize different transport regimes using the clustering
271 approach outlined in Sturm et al. (2013). This allowed us to distinguish among six different source
272 regions: Free Troposphere (FT), Southwest (SW), East (E), Local (L), West (W) and Northwest
273 (NW).

274 Similar to Henne et al. (2016) for CH_4 and based on spatially resolved N_2O emission inventories
275 (Meteotest for Switzerland; EDGAR for Europe), we used the FLEXPART concentration
276 footprints to calculate time-series of atmospheric mole fraction increases at Jungfraujoch resolved
277 by emission sectors (Henne et al., 2016). The emission inventory by Meteotest consists of 12
278 emission sectors, among which all sectors except “organic soils” are comparable to sectors in the
279 EDGAR inventory (See Table [S2S1](#)) (Janssens-Maenhout et al., 2019). To improve seasonal
280 representation of the emissions in our model, we used a monthly resolved, optimized version of
281 the emission inventory, which was obtained through inverse modeling using the N_2O atmospheric
282 mole fractions observed between March 2017 and September 2018 at the tall tower site

283 Beromuenster on the Swiss plateau (Henne et al., 2019). Therefore, in this study, source
284 contributions to Jungfraujoch were estimated specifically for the period mentioned above.

285 **2.6 Evaluation of seasonal pattern and interannual trend for time-series**

286 To explore seasonality and interannual trends, we fit the time-series of *in situ* measurements of
287 N₂O and O₃ mixing ratios, NO_y-to-CO ratios and isotopic measurements of N₂O with polynomial
288 functions and Fourier series (four harmonics for *in situ* measurements and two harmonics for
289 discrete measurements) (Thoning et al., 1989). Time-series were then decomposed into a linear
290 trend, seasonal variability (per 12 months) and residuals. This fit was conducted with a nonlinear
291 least-squares (NLS) model with R-3.5.3 (R Core Team, 2016). The detrended seasonality was
292 examined by comparing peak-to-peak amplitudes with our analytical precisions and the
293 uncertainty given by the one standard deviation of monthly residuals. To determine interannual
294 trends, a linear regression was applied to both the raw and the deseasonalized datasets. The
295 significance level is set to $p < 0.01$. The interannual trends for N₂O mixing ratios were found to be
296 little affected by seasonality, so growth rates were determined only based on the raw datasets.

297 Although Jungfraujoch is a remote site, episodic influence from the planetary boundary layer can
298 be observed at the station (Pandey Deolal et al., 2012; Zellweger et al., 2003). For evaluating trends
299 of N₂O mixing ratio measurements, we filtered out *in situ* data with significant influence of plenary
300 boundary layer, in order to represent a major air mass footprint from the free troposphere (FT). In
301 addition to the air transport regimes, an alternative filtering criteria for the free troposphere was
302 based on the published mean ranges of NO_y mixing ratios (501-748 pmol mol⁻¹ ppt depending on
303 the season) and NO_y to CO ratios (0.003-0.005 depending on the season) at Jungfraujoch
304 (Zellweger et al., 2003). This criterion is less strict than that given by footprint analyses (Herrmann

305 et al., 2015). After applying this criterion to the isotopic time-series (which led to the exclusion of
306 32 measurement points), we re-evaluated the seasonal and interannual trends in the N₂O isotopic
307 composition. In addition, because of the strong variability observed for isotopic data during the
308 first 1.5 years (until February 2016), we performed an independent evaluation for the time-series
309 starting from August 2016.

310 **2.7 Two-box model simulation**

311 A two-box model representing a well-mixed troposphere and stratosphere was used to estimate the
312 anthropogenic N₂O source strength and isotopic composition from the trends measured at
313 Jungfraujoch, similar to the approaches used by several previous studies (Ishijima et al., 2007;
314 Röckmann et al., 2003; Schilt et al., 2014; Sowers et al., 2002). The input variables used to run the
315 model are given in Table [S4S2](#). 200 iterations of the model were run using a Monte Carlo-style
316 approach to approximate the uncertainty considering the uncertainty distribution for each input
317 variable as given in Table [S4S2](#). All variables were set independently within the Monte Carlo
318 approximation except for preindustrial N₂O life time (τ_{PI}), which was fixed to 106% of the
319 present-day N₂O life time τ_{PD} (Prather et al., 2015).

320 Within each iteration of the model, the preindustrial N₂O burden was first described, assuming
321 steady state in the preindustrial era. The preindustrial stratospheric N₂O mixing ratio ($c_{S,PI}$)
322 (270 ± 7.5 nmol mol⁻¹) was taken from Sowers et al. (2002):

$$323 \quad 0 = TSF_{ex} (c_{PI} - c_{S,PI}) - (M_{PI} + M_{S,PI})/\tau_{PI} \quad (4)$$

324 where $TS_{ex}F_{ex}$ refers to the troposphere-stratosphere exchange rate; c_{PI} refers to the preindustrial
325 tropospheric N₂O mixing ratio; and M_{PI} and $M_{S,PI}$ are the masses of N₂O in the troposphere and
326 stratosphere respectively. The preindustrial terrestrial flux in Sowers et al. (2002) (equation 2) was

327 used here assuming no anthropogenic emissions. The delta values for the preindustrial stratosphere
328 and the fractionation factor for the stratospheric sink were taken from equations 6 and 7 from
329 Sowers et al. (2002) assuming steady state and no anthropogenic emissions. The model was run
330 with a yearly time step starting from the preindustrial assuming that anthropogenic emissions
331 began in 1845 (Sowers et al., 2002). For each year of the model run, the anthropogenic flux was
332 calculated according to the exponential increase described by Sowers et al. (2002):

$$333 \quad F_{\text{anth},t} = e^{\alpha(t-t_0)} - 1 \quad (5)$$

334 where t is the current year, $t_0 = 1845$ and α is the growth rate (assumed to be constant). The rates
335 of change for tropospheric and stratospheric N₂O mixing ratios were then retrieved from equations
336 2 and 3 in Sowers et al. (2002), and for the isotopic composition of stratospheric and tropospheric
337 N₂O from equations 6 and 7 in Sowers et al. (2002).

338 The values of the parameters describing the anthropogenic flux were optimized to fit both the trend
339 and the absolute values for the five years of Jungfraujoch isotope data, and the mixing ratio data
340 from the Jungfraujoch flasks and *in situ* data since 2005 (GAW data source). The uncertainties in
341 α and in the anthropogenic source isotopic signatures were approximated by one standard
342 deviation of values derived from repeated model runs.

343 2.8 Evaluation of the combined effects from STE and soil emission on $\delta^{15}\text{N}^{\text{SP}}$

344 To evaluate the combined effects of STE and soil emission on the seasonal variability of $\delta^{15}\text{N}^{\text{SP}}$
345 (i.e. August minima), we made a mixing calculation as below:

346 Soil emission: Based on the determined seasonality of N₂O mole fraction at Jungfraujoch, the
347 maximum N₂O mole fraction enhancement was approximately 0.2 nmol mol⁻¹ above baseline (Fig.

348 1b). Hence, we assumed N₂O enhancement from soil emission to be close to 0.15 to 0.20 nmol
349 mol⁻¹, which is close to the maximum N₂O enhancement in our observation. The isotopic effect
350 from soil emission can be derived from the difference between soil emission (7.2‰; Table S1) and
351 tropospheric air (18‰, Fig. 2) in $\delta^{15}\text{N}^{\text{SP}}$, i.e. -10.8‰.

352 *Mixing with stratospheric air:* The minimum of N₂O mole fraction in August (-0.20 nmol mol⁻¹)
353 is likely to be the result of both N₂O mole fraction enhancement from soil emission and N₂O mole
354 fraction depletion due to STE. Given the assumed N₂O enhancement from soil emission, we
355 estimated the N₂O depletion due to STE as -0.35 to -0.40 nmol mol⁻¹. The isotopic effect due to
356 mixing with stratospheric air can be approximated using the apparent isotopic fractionation ϵ_{app}
357 (Kaiser et al., 2006), which was derived from the slope of Rayleigh plot with normalized N₂O
358 mole and isotope ratios. For $^{15}\text{N}^{\text{SP}}$, ϵ_{app} is calculated from the difference between $^{15}\text{N}/^{14}\text{N}$ isotope
359 fractionations at the central and terminal N atoms, i.e. $\alpha_{\text{app}} - \beta_{\text{app}}$. Therefore, for the lower
360 stratosphere, $\epsilon_{\text{app}}(^{15}\text{N}^{\text{SP}})$ was calculated to be about -15‰ (see more details in Kaiser et al., 2006).

361 *Overall effect:* Combing the isotope effects and contributions to the change of N₂O mole fraction
362 by the two processes, the net effect is $[(-0.35 \text{ to } -0.40 \text{ nmol mol}^{-1}) (-15\text{‰}) + (0.15 \text{ to } 0.20 \text{ nmol}$
363 $\text{mol}^{-1}) (-10.8\text{‰})] / (330 \text{ nmol mol}^{-1}) \approx 0.01\text{‰}$. Such isotope effect is below our analytical
364 precision and too small to be measured in the background atmosphere.

365 **2.8.9 “Bottom-up” estimates of source isotopic signatures**

366 To gauge the accuracy of the two-box model, we deployed a “bottom-up” approach as an
367 alternative method of estimating the N₂O source signatures. The isotopic signatures of most N₂O
368 source sectors given in the Meteotest/EDGAR emission inventory are available from the literature,
369 except for the “Refinery” (Table [S2S1](#)). As “Refinery” generally contributes only about 0.02% of

370 the N₂O emission at Jungfraujoch, it was excluded for source isotopic signature estimation. The
371 simulated N₂O emissions by variable sources were categorized according to the EDGAR emission
372 types (Janssens-Maenhout et al., 2019). We then calculated isotopic signatures for the overall
373 source and the anthropogenic sources alone (excluding indirect natural emission) as weighted
374 averages.

375 **3 Results**

376 **3.1 Atmospheric N₂O mixing ratios at Jungfraujoch**

377 We observed a linear growth of atmospheric N₂O at Jungfraujoch during the period 2014-2018
378 (Fig. 1a). A point-to-point comparison of discrete and *in situ* measurements showed good
379 agreement, in particular ~~for the second half of the study~~ after the first year (2016-2015-2018), where
380 the data quality of *in situ* measurements was largely improved due to the implementation of the
381 more precise laser spectroscopy method as compared to GC-ECD (Fig. S3). The improvement in
382 analytical precision for N₂O mixing ratio was due to better temporal coverage by the OA-ICOS
383 instrument, in contrast with the GC analyses which conduct one measurement per 24-30 minutes.
384 The annual growth rates from 2014 to 2018 determined with *in situ* measurements were $0.880 \pm$
385 0.001 and 0.993 ± 0.001 nmol mol⁻¹ a⁻¹ with and without GC-ECD measurements in 2014,
386 respectively. ~~Such~~ This difference in N₂O growth rates is probably due to the limited data quality
387 of GC-ECD, although a lower growth rate in 2014 compared to 2015-2018 cannot be excluded due
388 to switch of analytical method suggests that analytical uncertainty in N₂O mixing ratios can
389 significantly influence its linear trends. -It is noteworthy that the N₂O growth ~~These~~ rates
390 determined for 2015 to 2019 at Jungfraujoch is slightly above ~~-are in agreement with~~ the global
391 mean growth rate for the recent decade reported by NOAA (0.93 ± 0.03 nmol mol⁻¹ a⁻¹) (WMO,
392 2018). If we filter the *in situ* dataset to examine only the “free troposphere” periods, we obtain a
393 lower increase (0.858 ± 0.002 nmol mol⁻¹ a⁻¹). By comparison, the absolute annual ~~growth rate~~
394 determined from the discrete gas samples was even lower albeit larger uncertainty (0.813 ± 0.027
395 nmol mol⁻¹ a⁻¹).

396 A significant seasonal pattern was observed for N₂O mixing ratios measured *in situ*, with a
397 maximum in early summer and a minimum in late summer (Fig. 1b). For discrete N₂O

398 measurements a similar trend was observed, but the detrended seasonality was not significant,
399 which might be due to the much lower number of samples (Fig. S4).

400 **3.2 Interannual trends of N₂O isotopic composition and anthropogenic source signatures**

401 Time-series of $\delta^{15}\text{N}^{\text{bulk}}$, $\delta^{15}\text{N}^{\text{SP}}$ and $\delta^{18}\text{O}$ for atmospheric N₂O at Jungfraujoch are shown in Figure
402 2. The NLS model simulation accounts well for the variabilities of isotopic time-series. Interannual
403 trends of three isotopic deltas were determined for both raw and deseasonalized datasets by linear
404 regression (Table 1). The deseasonalized interannual trends were slightly smaller than the trends
405 determined with the raw datasets. For the whole dataset, the deseasonalized trend indicates a
406 significant decrease in $\delta^{15}\text{N}^{\text{bulk}}$, of $-0.052\pm 0.012\text{‰ a}^{-1}$. In contrast, deseasonalized time-series of
407 $\delta^{15}\text{N}^{\text{SP}}$ and $\delta^{18}\text{O}$ increased, albeit insignificantly, by $0.065\pm 0.027\text{‰ a}^{-1}$ and $0.019\pm 0.011\text{‰ a}^{-1}$,
408 respectively. The trends determined for periods with major air mass footprints from the free
409 troposphere were close to those calculated for the whole dataset, except that $\delta^{15}\text{N}^{\text{SP}}$ trends
410 decreased after filtering out the samples with significant impact from plenary boundary layer. This
411 indicates that N₂O interannual trends observed at Jungfraujoch are of regional relevance, despite
412 the fact that a small impact from local sources can be seen. Because of the observed irregular
413 variability and the change in sampling frequency (though no change in daily sampling time) in our
414 dataset, we separated the time-series into two phases: April 2014-February 2016 (first phase;
415 weekly sampling) and August 2016-December 2018 (second phase; bi-weekly sampling). In the
416 first phase, the rates of increase in $\delta^{15}\text{N}^{\text{SP}}$ and $\delta^{18}\text{O}$ were almost one order of magnitude larger than
417 over the whole dataset. This is most likely due to the unexpectedly low $\delta^{15}\text{N}^{\text{SP}}$ and $\delta^{18}\text{O}$ in summer
418 2014 followed by a distinct increase in winter 2014-2015, which results in large rates of increase
419 over short periods. Such growth rates were not seen in the second phase, when both $\delta^{15}\text{N}^{\text{SP}}$ and

420 $\delta^{18}\text{O}$ showed small and insignificant variations. $\delta^{15}\text{N}^{\text{bulk}}$ displayed a decreasing interannual trend
421 in both phases; however, the rate of decrease was larger in the second phase ($-0.130\pm 0.045\% \text{ a}^{-1}$).
422 We tuned our two-box model to best match the observed N_2O mixing ratios and isotopic
423 composition at Jungfraujoch. An estimate of anthropogenic emissions and source signatures is
424 given in Table 2. For 2018, annual N_2O emissions were estimated to be $8.6\pm 0.6 \text{ Tg N}_2\text{O-N a}^{-1}$
425 equivalents. The average isotopic signatures for anthropogenic sources were $-8.6\pm 4\%$, $34.8\pm 3\%$
426 and $10.7\pm 4\%$ for $\delta^{15}\text{N}^{\text{bulk}}$, $\delta^{15}\text{N}^{\text{SP}}$ and $\delta^{18}\text{O}$, respectively, which are clearly lower than those for
427 preindustrial N_2O in the tropospheric background (Table [S4S2](#); Toyoda et al., 2013).

428 **3.3 Seasonal variation of N_2O isotopic composition**

429 $\delta^{15}\text{N}^{\text{SP}}$ of N_2O showed the most pronounced variability among all isotopic time-series (Fig. 2),
430 spanning 2.5% for individual flask sample measurements. Seasonal variability was estimated with
431 the NLS model and presented as mean seasonal cycles (Fig. 3). For $\delta^{15}\text{N}^{\text{SP}}$ a “summer minimum”
432 was found regardless of whether the entire dataset or only the second phase was considered (Fig.
433 3), although seasonal variability of the second time-series was smaller and showed the minimum
434 occurring earlier. The seasonal pattern of $\delta^{15}\text{N}^{\text{bulk}}$ determined from the whole dataset indicates a
435 significant summer maximum, but this was not seen when only the data from the second phase
436 was taken, as there was no significant seasonal pattern over this period alone. For $\delta^{18}\text{O}$, we
437 observed only small temporal variability and a lack of seasonal pattern. In addition, seasonal
438 variations of time-series filtered for free troposphere were evaluated; these show temporal patterns
439 similar to the whole dataset (Fig. S5).

440 **3.4 Air mass origin and *in situ* measurements at Jungfraujoch**

441 Back-trajectory simulations indicate six major transport clusters during 2014-2018, as shown in
442 Figure 4a. Four of these transport regimes (SW, E, L and NW) dominate, accounting for about 60-
443 90% coverage of the whole period. By contrast, the free troposphere cluster only represents 10-
444 20% of the data. Averaged monthly contributions of transport clusters are shown in Figure 4b,
445 with more pronounced impact by the L, E and NW regions in summer and stronger contribution
446 by FT and SW in winter. The source patterns of the air masses at Jungfraujoch were generally
447 consistent across the years in the present study. However, an apparent discrepancy was found for
448 discrete sampling times in the last two years (e.g. particularly low contribution from SW) which
449 is most likely due to the low and variable sampling frequency of the discrete sample collection
450 (Fig. 4b).

451 The detrended seasonal variability of *in situ* measurements indicates summer maxima for O_3 and
452 NO_y mixing ratios as well as NO_y -to-CO ratios at Jungfraujoch (Fig. S6). This likely indicates
453 stronger exchange with the polluted planetary boundary layer in summer ([Herrmann et al., 2015;](#)
454 [Zellweger et al., 2003](#))([Tarasova et al., 2009](#)), which is consistent with the seasonal pattern of air
455 mass footprint derived from back-trajectory simulations. The late spring-to-summer maxima for
456 O_3 mixing ratios may be attributed to air mixing with stratosphere and/or planetary boundary layer,
457 similar to the findings from a previous study at Jungfraujoch (Tarasova et al., 2009). On the other
458 hand, CO shows a maximum in early spring and decreases in summer when its atmospheric
459 lifetime is shortest. Atmospheric O_3 , NO_y and CO measurements during our discrete sampling
460 periods also well represented seasonal variability shown for *in situ* measurements, except for 2016-
461 2017 where there was a five-month sampling gap (Fig. S6).

462 Comparisons of air mass footprints as well as O_3 , NO_y and CO mixing ratios between *in situ* and
463 discrete sampling indicate that the discrete sampling covers the main air source regions and

464 variabilities in local pollution/free troposphere fairly well (Fig. 4 and S6). In the second phase
465 (2016-2018), the less frequent sampling impedes evaluation of the seasonal and interannual
466 variabilities.

467 **3.5 Relationship between N₂O isotopic signatures and air mass footprints**

468 We categorized N₂O mixing ratio and isotopic signature time-series into subsets based on the six
469 air mass transport clusters. One-way ANOVA among clusters indicates that N₂O mixing ratios in
470 air masses originating from cluster L were significantly higher and those from clusters FT and W
471 were significantly lower than the others (Fig. S75). In accordance with the pattern found for mixing
472 ratios, $\delta^{15}\text{N}^{\text{SP}}$ and $\delta^{18}\text{O}$ were high for cluster FT, and low for cluster L. For $\delta^{15}\text{N}^{\text{bulk}}$, little difference
473 between transport clusters was detected.

474 **4 Discussion**

475 **4.1 Quality assurance of isotopic measurements**

476 This study reports the first results of background N₂O isotopic measurements based on a laser
477 spectroscopic technique. Benefiting from the preconcentration process, we achieved measurement
478 repeatability for a target gas of 0.10-0.20‰ for $\delta^{15}\text{N}^{\text{bulk}}$ and $\delta^{18}\text{O}$ (Fig. S2), which is comparable
479 to that of IRMS measurements of ambient atmosphere (Park et al., 2012; Prokopiou et al., 2017;
480 Röckmann et al., 2003; Toyoda et al., 2013). The long-term robustness of our technique is adequate
481 for disentangling both seasonal and interannual temporal variability as shown in Figure 2. In
482 particular, our ~~analytical~~ repeatability of target measurements for $\delta^{15}\text{N}^{\text{SP}}$ (0.15-0.25‰) appears to
483 be better than previous studies measuring background atmosphere or firm air (0.8‰, Park et al.,
484 2012; 0.3‰, Prokopiou et al., 2017; 0.3‰, Toyoda et al., 2013).

485 **4.2 Seasonal variabilities of atmospheric N₂O isotopic composition**

486 *In situ* measurements of N₂O mixing ratios showed a clear early summer maximum and late
487 summer minimum (Fig. 1). Such a seasonal pattern was previously found for a number of NOAA
488 and AGAGE sites analyzing long-term N₂O records in the NH (Jiang et al., 2007; Nevison et al.,
489 2011). One explanation of the late-summer minimum is a strong influence of the STE process in
490 this period, which transports N₂O-depleted but isotopically enriched air downward from the
491 stratosphere into the troposphere (~~Decock and Six, 2013~~ Park et al., 2012; Snider et al., 2015b).
492 During the late summer at Jungfraujoch, we find strong enrichment of ¹⁵N in atmospheric N₂O
493 according to the detrended seasonality for the whole dataset (Fig. 3). This is supported by a
494 FLEXPART model simulation of the contribution of upper tropospheric air to Jungfraujoch station,
495 showing highest contributions in August (Fig. S7; Henne et al., Personal Communication). At

496 Hateruma Island, Japan, Toyoda et al. (2013) observed a seasonal pattern of atmospheric N₂O
497 mixing ratios which is comparable almost identical to with our study, but found insignificant
498 variations of isotopic composition. On the other hand, N₂O seasonal variability could be influenced
499 by oceanic emission sources (Jiang et al., 2007; Nevison et al., 2005), complicating the underlying
500 mechanisms explanations for the observed temporal patterns. For example, in another study
501 looking at archived air from Cape Grim, Australia, Park et al. (2012) detected an April-May
502 minimum and a November-December maximum for N₂O. This is expected for the SH, as STE is
503 most prevalent in April (Nevison et al., 2011). They observed negative correlations of $\delta^{15}\text{N}^{\text{bulk}}$,
504 $\delta^{15}\text{N}^{\alpha}$ and $\delta^{18}\text{O}$ with N₂O mixing ratios, appearing to support the idea that the STE process is
505 responsible for seasonal variabilities in N₂O mixing ratios and isotopic composition at Cape Grim.
506 However, the seasonal cycle for $\delta^{15}\text{N}^{\alpha}$ was much larger than $\delta^{15}\text{N}^{\text{bulk}}$ and $\delta^{18}\text{O}$, which could not be
507 explained by STE alone. They suggested that the seasonal patterns of N₂O isotopes at Cape Grim
508 may be due to mixing between oceanic sources (high N₂O with low ¹⁵N and ¹⁸O) and STE (low
509 N₂O with high ¹⁵N and ¹⁸O) (Nevison et al., 2011; Park et al., 2012). However, because we
510 observed a concurrent minimum of $\delta^{15}\text{N}^{\text{SP}}$ and maximum of $\delta^{15}\text{N}^{\text{bulk}}$ in July-August with low N₂O
511 at Jungfraujoch (Fig. 3), additional mechanisms must be considered here.

512 Regional model simulations based on Swiss N₂O emissions derived from the inverse method were
513 used to explore contributions from different sources to the variability in N₂O enhancements at
514 Jungfraujoch. As shown in Figure 5a6a&6b, soil emissions, including direct and indirect emissions
515 from agricultural lands and emissions from (semi-)natural areas, account for more than 70% of the
516 total N₂O enhancements, while manure and waste management contribute another 20%. Total N₂O
517 enhancements appeared to be highest in May to July (Fig. 5e6c), in accordance with the highest
518 contribution by soil emissions. The early-to-middle summer maximum in the simulated N₂O

519 enhancements is comparable with maximum of N₂O mixing ratios in early summer as observed at
520 Jungfrauoch (Fig. 1b). This underlines the importance of soil emission in accounting for
521 atmospheric N₂O variability (Saikawa et al., 2014). In late summer, the minimum of $\delta^{15}\text{N}^{\text{SP}}$ (Fig.
522 3) may be then attributed to the influence of soil emitted N₂O, which has lower $\delta^{15}\text{N}^{\text{SP}}$ ($7.2\pm 3.8\text{‰}$;
523 Table S1) than the troposphere (Fig. 2). However, the STE process, which resulted in the minimum
524 of N₂O mixing ratio, likely contributes a positive isotope effect in the meanwhile (Kaiser et al.,
525 2006). In order to evaluate the combined effect of STE and soil emission on $\delta^{15}\text{N}^{\text{SP}}$ in late summer,
526 we applied a mixing calculation. Such estimate was made based on the approximated N₂O
527 enhancement/depletion contributed by the two processes and the assumed isotope effects (see more
528 details in M&M). The mixing calculation indicated an overall isotope effect of about 0.01‰, which
529 is extremely small and below our analytic precision. This practice suggests that it is still
530 challenging to build a direct link of N₂O sources/processes with the observed isotope signature in
531 the background atmosphere. It is also noteworthy that the $\delta^{15}\text{N}^{\text{SP}}$ used in the calculation ($7.2\pm 3.8\text{‰}$)
532 may underestimate the isotope effects of soil emission, given that denitrification, as a major N₂O
533 process in soils, produces N₂O with $\delta^{15}\text{N}^{\text{SP}}$ close to 0‰. ~~Soil N₂O emissions are mainly derived~~
534 ~~from denitrification and nitrification, which prevail in anaerobic and aerobic soil environment,~~
535 ~~respectively (Butterbach-Bahl et al., 2013). Denitrification-derived N₂O is expected to be about~~
536 ~~30‰ lower in $\delta^{15}\text{N}^{\text{SP}}$ than N₂O produced by nitrification (Sutka et al., 2006). Previous field studies~~
537 ~~at Swiss grasslands have demonstrated that low- $\delta^{15}\text{N}^{\text{SP}}$ N₂O emissions ($\sim 0\text{‰}$), i.e. following the~~
538 ~~denitrification pathway, dominates peak N₂O fluxes observed in summer periods predominates~~
539 ~~during summer periods at Swiss (Wolf et al., 2015) and German (Ibraim et al., 2019) grasslands.~~
540 ~~(Ibraim et al., 2019). On the other hand, the STE process is likely to exert a much smaller isotopic~~
541 ~~effect on the tropospheric N₂O (Toyoda et al., 2018). By estimating the contributions of two~~

542 ~~processes to N₂O enhancement/depletion in the late summer, we calculated the combined isotopic~~
543 ~~effects of both processes (see more details in the supplementary material), indicating that the~~
544 ~~negative effect of soil N₂O emission on $\delta^{15}\text{N}^{\text{SP}}$ likely outcompetes the positive effect by STE.~~
545 ~~Therefore, we hypothesize that the observed minimum of $\delta^{15}\text{N}^{\text{SP}}$ in late summer at Jungfrauoch~~
546 ~~is largely contributed by the prevailing N₂O production by denitrification.~~ By contrast, the
547 influence of biogeochemical processes (nitrification and denitrification) on $\delta^{15}\text{N}^{\text{bulk}}$ is generally
548 smaller than that on $\delta^{15}\text{N}^{\text{SP}}$ (Toyoda et al., 2011), and such effect on $\delta^{15}\text{N}^{\text{bulk}}$ are usually overwritten
549 by the wide range of isotopic signatures in soil N substrates (Sutka et al., 2006). Hence, given the
550 distinct $\delta^{15}\text{N}^{\text{bulk}}$ maximum and N₂O minimum in late summer during our observation (Figs. 1 and
551 3), we suggest that the STE process is mainly responsible for the seasonal variability in $\delta^{15}\text{N}^{\text{bulk}}$.

552 The footprint analyses based on air mass residence time revealed a seasonal pattern, with a higher
553 contribution of background air from the FT and SW regions in winter and more pronounced
554 contribution of local planetary boundary layer air from the L, E and NW regions in summer (Fig.
555 4b). The higher frequency of air mass footprints recently in contact with the surface in summer is
556 consistent with inverse modeling results, indicating a larger contribution of soil N₂O emissions in
557 June/July (Fig. [56](#)). For the air mass regime representing the free troposphere, N₂O mixing ratios
558 observed at Jungfrauoch were significantly below the average, while $\delta^{15}\text{N}^{\text{SP}}$ and $\delta^{18}\text{O}$ were higher
559 (Fig. [57](#)). By contrast, the local cluster (L) representing a strong impact from the planetary
560 boundary layer had higher N₂O mixing ratios and lower isotopic signatures (except $\delta^{15}\text{N}^{\text{bulk}}$) than
561 the other source regions. In addition, the ratios of NO_y to CO, which is a more ~~straight-~~
562 ~~forward~~straightforward indicator of the free troposphere (Zellweger et al., 2003), show significant
563 negative correlations with $\delta^{15}\text{N}^{\text{SP}}$ and $\delta^{18}\text{O}$, but not with $\delta^{15}\text{N}^{\text{bulk}}$ (Fig. S8). This further suggests
564 that the seasonal variability of $\delta^{15}\text{N}^{\text{SP}}$ and $\delta^{18}\text{O}$ observed at Jungfrauoch is most likely influenced

565 by ground-derived emissions, while fluctuations in N₂O mixing ratios and $\delta^{15}\text{N}^{\text{bulk}}$ are possibly
566 driven by STE.

567 Considering the complexity in mechanisms responsible for N₂O isotopic variations, we strongly
568 recommend more field measurements of N₂O isotopic signatures at higher frequency and at
569 different background sites, in order to cover spatial and temporal variability in N₂O sources. For
570 example, in the second phase, we only detected~~only~~ a significant seasonality of $\delta^{15}\text{N}^{\text{SP}}$, with a
571 minimum in July, which is one month earlier than the summer minimum found for the whole
572 dataset (Fig. 3). This may be attributed to a difference in source regions, as~~that~~ Northwest regions
573 appeared to be significantly more important during 2017 (second phase). However, due to low
574 sampling frequency, it is challenging to overcome the large uncertainty in seasonality analysis for
575 a two-year period such as the second phase.~~Also, the uncertainty in seasonal patterns could be~~
576 ~~further reduced by longer and more frequent isotopic measurements~~ ~~in situ monitoring at~~
577 ~~background sites like Jungfraujoch could be especially useful.~~

578 Based on our bottom-up approach, we simulated isotopic signatures for the overall N₂O sources
579 responsible for the N₂O mixing ratio increase in the atmosphere (Fig. S9). However, the
580 interpretation of simulated versus observed variability in N₂O isotopic composition was difficult,
581 except for the somewhat similar patterns in $\delta^{18}\text{O}$. Our results suggest a limitation in the current
582 knowledge and literature values on isotopic signatures of most N₂O sources. In addition, most N₂O
583 sources may not exhibit a well-defined isotopic signature but a range of values regulated under a
584 number of processes/environmental factors. For example, isotopic signatures of soil-derived N₂O
585 are often determined by an interaction of several soil and climatic factors. It might be possible in
586 the future to model these changes implementing isotopes in ecosystem models, as recently
587 demonstrated by Denk et al. (2019).

588 4.3 Interannual trends of atmospheric N₂O isotopic composition

589 Over a period of almost five years, our observations show an interannual increase in N₂O mixing
590 ratio and decrease in $\delta^{15}\text{N}^{\text{bulk}}$ (Fig. 67). This is to be expected, assuming that the atmospheric N₂O
591 increase is primarily attributed to anthropogenic sources, which emit isotopically lighter N₂O
592 relative to the tropospheric background (Table S2S1) (Rahn and Wahlen, 2000). Compared to
593 several studies on firn air (Ishijima et al., 2007; Röckmann et al., 2003) and surface air (Park et al.,
594 2012; Röckmann and Levin, 2005; Toyoda et al., 2013), the rate of decrease for $\delta^{15}\text{N}^{\text{bulk}}$ at
595 Jungfraujoch is relatively high (-0.05 to -0.06‰ a^{-1} , Table 1). Such a discrepancy in the $\delta^{15}\text{N}^{\text{bulk}}$
596 trend could be due to a large contribution of terrestrial N₂O emission from the European continent
597 to Jungfraujoch (Figs. 1 and 5), as N₂O originating from soil emissions is significantly more
598 isotopically depleted than that of oceanic sources (Snider et al., 2015b). Nevertheless, our
599 observation period is shorter than that of other studies, so the interannual trends determined here
600 are more likely affected by year-to-year variability. Among all reported records, the decrease of
601 $\delta^{15}\text{N}^{\text{bulk}}$ observed at Hateruma Island was the most up-to-date and smallest (-0.020-0.026‰ a⁻¹)
602 (Toyoda et al., 2013). The authors argued that the smaller declining trend for $\delta^{15}\text{N}^{\text{bulk}}$ may be
603 explained by the recent increase in anthropogenic isotopic ratios particularly for agricultural N₂O
604 emissions, although Ishijima et al. (2007) suggested a decline in both $\delta^{15}\text{N}^{\text{bulk}}$ and $\delta^{18}\text{O}$ in
605 anthropogenic N₂O from 1952-1970 to 1970-2001 based on inverse modeling.

606 For the interannual trends observed at Jungfraujoch, it is noteworthy to point out that our
607 observations covering a rather short period may lead to large uncertainties despite statistical
608 significance. The discrepancy found in the trends between the first and second phases indicates
609 that variability of N₂O isotopic composition is likely to obscure interannual trends over shorter
610 periods (Toyoda et al., 2013). Hence, extended time-series of isotopic measurements are needed

611 to reevaluate, for example, the observed tendency of increase in $\delta^{18}\text{O}$ and $\delta^{15}\text{N}^{\text{SP}}$ at Jungfraujoch
612 (Table 1; only significant during the first phase). For $\delta^{18}\text{O}$ of atmospheric N_2O , a generally
613 declining trend smaller than that of $\delta^{15}\text{N}^{\text{bulk}}$ has been indicated by a number of observations
614 (Bernard et al., 2006; Ishijima et al., 2007; Park et al., 2012; Röckmann et al., 2003; Röckmann
615 and Levin, 2005). This is expected as $\delta^{18}\text{O}$ of anthropogenic N_2O is not much different from that
616 of the natural background, given assuming that the oxygen atom in N_2O is largely derived from
617 soil water and ambient oxygen during production (Rahn and Wahlen, 2000).

618 It is still a challenging task to disentangle interannual trends of $\delta^{15}\text{N}^{\text{SP}}\text{-N}_2\text{O}$ in the background
619 atmosphere, due to limitations in analytical repeatability and precision (Harris et al., 2017; Mohn
620 et al., 2014). Past results have reached inconsistent conclusions, showing positive (Bernard et al.,
621 2006; Park et al., 2012; Prokopiou et al., 2017; Röckmann and Levin, 2005) or negative
622 (Röckmann et al., 2003; Toyoda et al., 2013) trends of similar magnitude (Fig. 67). On the one
623 hand, the negative trend in $\delta^{15}\text{N}^{\text{SP}}$ could be explained by the significantly lower $\delta^{15}\text{N}^{\text{SP}}$ from
624 anthropogenic sources (e.g. agricultural sources; Table S2S1) than of the tropospheric background
625 (near 18‰; Fig. 67). On the other hand, Park et al. (2012) suggested that the increase of $\delta^{15}\text{N}^{\text{SP}}$ in
626 the atmospheric N_2O may reflect a global increase in importance of the contribution by nitrification
627 (high- $\delta^{15}\text{N}^{\text{SP}}$ process) to agricultural N_2O emissions. This is based on the assumption that the
628 growth of N_2O emissions is largely due to enhanced fertilizer application which promotes
629 nitrification activity (Pérez et al., 2001; Tian et al., 20198). The observed mean increase rate of
630 0.02‰ a^{-1} for $\delta^{15}\text{N}^{\text{SP}}$ by Park et al. (2012) could then be translated into an increase of 13-23% for
631 the relative amount of nitrification-derived N_2O between 1750 and 2005. However, this should be
632 further evaluated with more frequent sampling (Park et al. (2012) only sampled 1-6 times per year)
633 and tested with isotopic measurements across the NH, where agricultural N_2O emissions are more

634 dominant than in the SH. In addition, the strong seasonal pattern of $\delta^{15}\text{N}^{\text{SP}}$ at Jungfraujoch suggests
635 that seasonal variations of $\delta^{15}\text{N}^{\text{SP}}$ in response to climatic or source factors are crucial and must be
636 taken into consideration for evaluating interannual $\delta^{15}\text{N}^{\text{SP}}$ trends.

637 **4.4 Simulated anthropogenic N₂O sources with the two-box model and comparison with** 638 **other studies**

639 To further evaluate anthropogenic source signatures of N₂O isotopic composition, we applied a
640 two-box model representing a well-mixed troposphere and stratosphere (Röckmann et al., 2003;
641 Schilt et al., 2014; Sowers et al., 2002). The model runs with the whole dataset (Table 2) and the
642 dataset filtered for free-troposphere only dataset (Table 2)(Table S3) exhibit statistically identical
643 results, supporting that our model estimates, with observations at Jungfraujoch, isare
644 representative of the background atmosphere. The simulated trends of the N₂O mixing ratios and
645 isotopic composition show a gradual increase in N₂O and decrease in the isotopic signatures (see
646 Fig. 67), which agree with existing observations within the model uncertainty. However, this does
647 not hold for individual studies considered separately. For example, the N₂O mixing ratios observed
648 by Röckmann et al. (2003) and Prokopiou et al. (2017) would lead to a higher preindustrial N₂O
649 compared to our model simulation, which is likely due to the uncertainty in the firm air records
650 (Prokopiou et al., 2017).

651 We compared the anthropogenic isotopic signatures determined by our two-box model with other
652 similar studies in Table 2. Our estimates generally lie within the ranges given in the earlier studies
653 (Ishijima et al., 2007; Park et al., 2012; Prokopiou et al., 2017; Röckmann et al., 2003; Sowers et
654 al., 2002; Toyoda et al., 2013). However, isotopic signatures of N₂O sources estimated for 2018 in
655 this study are higher in $\delta^{15}\text{N}^{\text{bulk}}$ and $\delta^{18}\text{O}$ (by 4-8‰), and lower in $\delta^{15}\text{N}^{\text{SP}}$ (by 2-7‰) than model
656 estimates for the early 2000s from two other studies from SH (Park et al., 2012; Prokopiou et al.,

2017). Such differences in $\delta^{15}\text{N}^{\text{bulk}}$ and $\delta^{18}\text{O}$ could be related to interhemispheric differences, as the relative contributions of N_2O sources vary between the two hemispheres (Toyoda et al., 2013). Also, more interestingly, this could suggest a shift in the N_2O source isotopic signatures over the last few decades. For example, an increase of $\delta^{15}\text{N}^{\text{bulk}}$ in anthropogenic N_2O sources over time may be attributed to growing contributions of other industrial/waste sources with high $\delta^{15}\text{N}^{\text{bulk}}$ (Prokopiou et al., 2017). In addition, if the assumption of increasing $\delta^{15}\text{N}^{\text{bulk}}$ and decreasing $\delta^{15}\text{N}^{\text{SP}}$ in anthropogenic N_2O sources over time holds, it points to a recently growing contribution of denitrification relative to nitrification, to the global atmospheric N_2O increase (Sutka et al., 2006; Toyoda et al., 2013). ~~This does not necessarily contradict~~ By contrast, Park et al. (2012) ~~or and~~ Prokopiou et al. (2017), ~~who~~ proposed an increasing importance of nitrification for anthropogenic N_2O emissions based on the increasing $\delta^{15}\text{N}^{\text{SP}}$ trend since 1940, ~~-. This may suggest as that the change in N_2O source processes in recent decades may instead reflect~~ a stronger climate change feedback has recently resulted in significant shifts in N_2O source process, hence twisting the isotopic signatures of anthropogenic sources (Griffis et al., 2017; Xu-Ri et al., 2012). Alternatively, the uncertainty in determining N_2O isotopic signatures in the background atmosphere and inter-laboratory comparability may play a role in the observed discrepancy.

Given the strong heterogeneity in source contributions to N_2O emissions around the globe (Saikawa et al., 2014), current two- and four-box model estimates based on observations at individual sites or regions are likely to reflect latitudinal or even interhemispheric differences in anthropogenic isotopic signatures. On the other hand, previous discussions of the model sensitivities by Röckmann et al. (2003) and Toyoda et al. (2013) have suggested that anthropogenic isotopic values are most sensitive to the trends in tropospheric isotopic values ~~as well as and~~ the relative difference in tropospheric isotopic values between present and preindustrial times. ~~As~~

680 ~~shown in Figure 6~~For example, given the similar parameters used for preindustrial times as our
681 ~~study~~, Park et al. (2012) observed much lower $\delta^{15}\text{N}^{\text{bulk}}$ in the recent troposphere than in our case,
682 hence resulting in significantly lower $\delta^{15}\text{N}^{\text{bulk}}$ for the anthropogenic source. Furthermore, and both
683 Park et al. (2012) and Prokopiou et al. (2017) ~~found~~ simulated a positive trend in $\delta^{15}\text{N}^{\text{SP}}$ relative
684 to preindustrial times, which in return computed resulted in a much higher $\delta^{15}\text{N}^{\text{SP}}$ for the
685 anthropogenic sources. These may help to explain some differences in anthropogenic source
686 signatures between our and their box model estimates.

687 Using an alternative bottom-up approach, we estimated the anthropogenic source isotopic
688 signatures based on the N₂O emission inventory simulated for Jungfraujoch and published source
689 isotopic signatures as summarized by Harris et al. (2017) (Table [S2S1](#)). The retrieved
690 anthropogenic isotopic signatures (Table 3) were largely in agreement with the isotopic signature
691 of agricultural soil emissions (Snider et al., 2015b; Wolf et al., 2015), indicating that this source
692 could explain more than 60% of the total N₂O emissions. However, the anthropogenic isotopic
693 signatures estimated by this approach were lower than the results from our two-box model (Table
694 2). In contrast, another similar bottom-up estimate based on the global N₂O emission inventory
695 (Toyoda et al., 2013) reported anthropogenic isotopic values that agree well with our box-model
696 results. This may be explained by the different isotopic signatures used to describe agricultural
697 N₂O emissions, as those values used for the bottom-up estimates by Toyoda et al. (2013) were
698 significantly lower (Toyoda et al., 2011) than those used in this study (Snider et al., 2015b; Wolf
699 et al., 2015). Such bottom-up estimation suggests that more isotopic measurements of the
700 background atmosphere from different regions, and better constraints on individual anthropogenic
701 (especially agricultural) N₂O isotopic signatures, are necessary for a better representation of N₂O
702 isotopic composition in atmospheric modeling studies.

703 **5 Conclusions**

704 With the recently developed laser spectroscopic technique coupled with a preconcentration device,
705 we achieved good repeatability in measurements of N₂O isotopic composition from the
706 background atmosphere at Jungfraujoch, Switzerland. This time-series covered a period of five
707 years and showed a distinct seasonality, with $\delta^{15}\text{N}^{\text{bulk}}$ maxima and $\delta^{15}\text{N}^{\text{SP}}$ minima in late summer,
708 associated with the lowest N₂O mixing ratios over the year. The seasonal fluctuation of $\delta^{15}\text{N}^{\text{bulk}}$
709 was associated with the stratosphere-troposphere exchange process, in agreement with other
710 monitoring networks (Nevison et al., 2011), while the contrasting depletion of $\delta^{15}\text{N}^{\text{SP}}$ in later
711 summer is possibly a combined result of STE and agricultural emissions, with the latter being more
712 important. The analyses of air mass transport regimes together with the simulation of N₂O
713 enhancements for Jungfraujoch supported our explanations and highlighted that the fluctuation
714 between the free troposphere and local contributions dominated by soil emission drives the
715 seasonality of $\delta^{15}\text{N}^{\text{SP}}$ and $\delta^{18}\text{O}$ as observed at Jungfraujoch.

716 We found statistically significant interannual trends for $\delta^{15}\text{N}^{\text{bulk}}$, which is expected as
717 anthropogenic N₂O sources are characterized by low ¹⁵N abundance. For $\delta^{15}\text{N}^{\text{SP}}$ and $\delta^{18}\text{O}$,
718 interannual trends were highly uncertain and possibly masked by ~~higher frequency~~ their large
719 temporal variability~~tion~~. Using a two-box model approach, we simulated the evolution of N₂O
720 isotopic composition from preindustrial times to the present. This model suggests an overall
721 decreasing trend for all isotopic deltasspecies in conjunction with the atmospheric N₂O increase.
722 The anthropogenic source signatures given by the model generally agreed with previous studies.
723 However, these model results are still sensitive to the ranges and trends of the observed N₂O
724 isotopic signatures in the present troposphere. In the future, more extended records of high-
725 precision N₂O isotopic measurements and application of multiple-box modeling approaches

726 (Rigby et al., 2013) are necessary to account for the global N₂O budget and evolution of
727 anthropogenic sources.

728 **Data availability**

729 ~~Data for this study have been deposited in a general data repository~~
730 ~~(<https://figshare.com/s/077562ab408dd1bd0880>; doi:10.6084/m9.figshare.12032760.v1, 2020).~~
731 ~~for N₂O mixing ratios and isotopic composition of flask samples at Jungfraujoch could be found~~
732 ~~in the supplementary materials. *In situ* data for N₂O mixing ratios at Jungfraujoch are available~~
733 ~~from World Data Centre for Greenhouse Gases (WMO-GAW; <https://gaw.kishou.go.jp>).~~ Other
734 ~~data are available upon request through the corresponding author (longfei.yu@empa.ch).~~

735 **Author contribution:**

736 LY, EH and JM led and designed this study. LY, EH, SE conducted sample collection at
737 Jungfraujoch; LY and EH analyzed discrete samples at Empa; MS and CZ contributed *in situ*
738 measurements of N₂O, NO_y, CO and O₃ at Jungfraujoch; LY, EH and SH performed data analyses
739 for the time-series and conducted model simulations. LY wrote the main manuscript; EH, SH and
740 JM were involved in the revisions of the manuscript and commenting. SE, MS, LE and CZ were
741 also involved in scientific discussion and commenting on the manuscript.

742 **Competing interests**

743 The authors declare that they have no conflict of interest.

744 **Acknowledgements**

745 We are thankful to the research infrastructure provided by the High Altitude Research Stations
746 Jungfraujoch and Gornergrat. We are grateful to the help from the custodians (Mr. and Mrs. Fischer
747 and Mr. and Mrs. Käser) at the research station of Jungfraujoch. We would like to thank Simon
748 Wyss, Kerstin Zeyer, Patrik Zanchetta and Flurin Dietz for their support with the sample collection
749 as well as laboratory assistance. The NABEL network is operated by Empa in collaboration with

750 the Swiss Federal Office for the Environment. Prof. Sakae Toyoda and Prof. Naohiro Yoshida
751 from Tokyo Institute of Technology are acknowledged for their analyses of the applied reference
752 standards. This study was financially supported by the Swiss National Science Foundation (grant
753 number 200021_163075) and the Swiss contribution to the Integrated Carbon Observation System
754 (ICOS) Research Infrastructure (ICOS-CH). ICOS-CH is funded by the Swiss National Science
755 Foundation and in-house contributions. Longfei Yu was additionally supported by the
756 EMPAPOSTDOCS-II program, which receives funding from the European Union's Horizon 2020
757 research and innovation program under the Marie Skłodowska-Curie grant agreement number
758 754364.

759

760 **References**

- 761 Appenzeller, C., Begert, M., Zenklusen, E. and Scherrer, S. C.: Monitoring climate at Jungfrauoch in the
762 high Swiss Alpine region, *Sci. Total Environ.*, 391(2–3), 262–268, doi:10.1016/j.scitotenv.2007.10.005,
763 2008.
- 764 Bernard, S., Röckmann, T., Kaiser, J., Barnola, J.-M., Fischer, H., Blunier, T. and Chappellaz, J.:
765 Constraints on N₂O budget changes since pre-industrial time from new firn air and ice core isotope
766 measurements, *Atmos. Chem. Phys. Discuss.*, 5(4), 7547–7575, doi:10.5194/acpd-5-7547-2005, 2006.
- 767 Bourbonnais, A., Letscher, R. T., Bange, H. W., Échevin, V., Larkum, J., Mohn, J., Yoshida, N. and
768 Altabet, M. A.: N₂O production and consumption from stable isotopic and concentration data in the
769 Peruvian coastal upwelling system, *Global Biogeochem. Cycles*, 31(4), 678–698,
770 doi:10.1002/2016GB005567, 2017.
- 771 Buchmann, B., Hueglin, C., Reimann, S., Vollmer, M. K., Steinbacher, M. and Emmenegger, L.: Reactive
772 gases, ozone depleting substances and greenhouse gases, in *From weather observations to atmospheric
773 and climate sciences in Switzerland*, edited by S. Willemse and M. Furger, vdf Hochschulverlag AG.,
774 2016.
- 775 Bukowiecki, N., Weingartner, E., Gysel, M., Coen, M. C., Zieger, P., Herrmann, E., Steinbacher, M.,
776 Gäggeler, H. W. and Baltensperger, U.: A review of more than 20 years of aerosol observation at the high
777 altitude research station Jungfrauoch, Switzerland (3580 m asl), *Aerosol Air Qual. Res.*, 16(3), 764–788,
778 doi:10.4209/aaqr.2015.05.0305, 2016.
- 779 Butterbach-Bahl, K., Baggs, E. M., Dannenmann, M., Kiese, R. and Zechmeister-Boltenstern, S.: Nitrous
780 oxide emissions from soils: how well do we understand the processes and their controls?, *Philos. Trans.
781 R. Soc. Lond. B. Biol. Sci.*, 368, 20130122, doi:10.1098/rstb.2013.0122, 2013.
- 782 Decock, C. and Six, J.: How reliable is the intramolecular distribution of ¹⁵N in N₂O to source partition
783 N₂O emitted from soil?, *Soil Biol. Biochem.*, 65(2), 114–127, doi:10.1016/j.soilbio.2013.05.012, 2013.
- 784 Denk, T. R. A., Mohn, J., Decock, C., Lewicka-Szczepak, D., Harris, E., Butterbach-Bahl, K., Kiese, R.
785 and Wolf, B.: The nitrogen cycle: A review of isotope effects and isotope modeling approaches, *Soil Biol.
786 Biochem.*, 105, 121–137, doi:10.1016/j.soilbio.2016.11.015, 2017.
- 787 Denk, T. R. A., Kraus, D., Kiese, R., Butterbach-Bahl, K. and Wolf, B.: Constraining N cycling in the
788 ecosystem model LandscapeDNDC with the stable isotope model SIMONE, *Ecology*, 100(5), c02675,
789 doi:10.1002/ecy.2675, 2019.
- 790 Fowler, D., Steadman, C. E., Stevenson, D., Coyle, M., Rees, R. M., Skiba, U. M., Sutton, M. a., Cape, J.
791 N., Dore, a. J., Viena, M., Simpson, D., Zaehle, S., Stocker, B. D., Rinaldi, M., Facchini, M. C.,
792 Flechard, C. R., Nemitz, E., Twigg, M., Erisman, J. W. and Galloway, J. N.: Effects of global change
793 during the 21st century on the nitrogen cycle, *Atmos. Chem. Phys. Discuss.*, 15(2), 1747–1868,
794 doi:10.5194/acpd-15-1747-2015, 2015.
- 795 Fujii, A., Toyoda, S., Yoshida, O., Watanabe, S., Sasaki, K. and Yoshida, N.: Distribution of nitrous
796 oxide dissolved in water masses in the eastern subtropical North Pacific and its origin inferred from
797 isotopomer analysis, *J. Oceanogr.*, 69(2), 147–157, doi:10.1007/s10872-012-0162-4, 2013.
- 798 Griffis, T. J., Chen, Z., Baker, J. M., Wood, J. D., Millet, D. B., Lee, X., Venterea, R. T. and Turner, P.
799 A.: Nitrous oxide emissions are enhanced in a warmer and wetter world, *Proc. Natl. Acad. Sci.*,
800 201704552, doi:10.1073/pnas.1704552114, 2017.
- 801 Hall, B. D., Dutton, G. S. and Elkins, J. W.: The NOAA nitrous oxide standard scale for atmospheric
802 observations, *J. Geophys. Res. Atmos.*, 112(9), 1–9, doi:10.1029/2006JD007954, 2007.

803 Harris, E., Ibraim, E., Henne, S., Hüglin, C., Zellweger, C., Tuzson, B., Emmenegger, L. and Mohn, J.:
804 Tracking nitrous oxide emission processes at a suburban site with semicontinuous, in situ measurements
805 of isotopic composition, *J. Geophys. Res. Atmos.*, 122, 1850–1870, doi:10.1002/2016JD025906, 2017.

806 Harris, E. J., Nelson, D. D., Olsewski, W., Zahniser, M., Potter, E., Mcmanus, B. J., Whitehill, A., Prinn,
807 R. G., Ono, S. and Harris, E.: Development of a spectroscopic technique for continuous online monitoring
808 of oxygen and site-specific nitrogen isotopic com, *Anal. Chem.*, 86(3), 1726–1734, 2014.

809 Heil, J., Wolf, B., Brüggemann, N., Emmenegger, L., Tuzson, B., Vereecken, H. and Mohn, J.: Site-
810 specific ^{15}N isotopic signatures of abiotically produced N_2O , *Geochim. Cosmochim. Acta*, 139, 72–82,
811 doi:10.1016/j.gca.2014.04.037, 2014.

812 Henne, S., Brunner, D., Folini, D., Solberg, S., Klausen, J. and Buchmann, B.: Assessment of parameters
813 describing representativeness of air quality in-situ measurement sites, *Atmos. Chem. Phys.*, 10(8), 3561–
814 3581, doi:10.5194/acp-10-3561-2010, 2010.

815 Henne, S., Brunner, D., Oney, B., Leuenberger, M., Eugster, W., Bamberger, I., Meinhardt, F.,
816 Steinbacher, M. and Emmenegger, L.: Validation of the Swiss methane emission inventory by
817 atmospheric observations and inverse modelling, *Atmos. Chem. Phys.*, 16(6), 3683–3710,
818 doi:10.5194/acp-16-3683-2016, 2016.

819 Henne, S., Mohn, J. and Brunner, D.: Quantification of Swiss nitrous oxide emissions through
820 atmospheric observations and inverse modelling, Final Report, Project of FOEN, 2019.

821 Herrmann, E., Weingartner, E., Henne, S., Vuilleumier, L., Bukowiecki, N., Steinbacher, M., Conen, F.,
822 Coen, M. C., Hammer, E., Juranyi, Z., Baltensperger, U. and Gysel, M.: Analysis of long-term aerosol
823 size distribution data from Jungfraujoch with emphasis on free tropospheric conditions, cloud influence,
824 and air mass transport, *J. Geophys. Res. Atmos.*, 120, 1751–1762, doi:10.1002/2015JD023660, 2015.

825 Ibraim, E., Wolf, B., Harris, E., Gasche, R., Wei, J., Yu, L., Kiese, R., Eggleston, S., Butterbach-Bahl, K.,
826 Zeeman, M., Tuzson, B., Emmenegger, L., Six, J., Henne, S. and Mohn, J.: Attribution of N_2O sources in
827 a grassland soil with laser spectroscopy based isotopocule analysis, *Biogeosciences*, 16, 3247–3266,
828 doi.org/10.5194/bg-16-3247-2019, 2019.

829 Ishijima, K., Sugawara, S., Kawamura, K., Hashida, G., Morimoto, S., Murayama, S., Aoki, S. and
830 Nakazawa, T.: Temporal variations of the atmospheric nitrous oxide concentration and its $\delta^{15}\text{N}$ and $\delta^{18}\text{O}$
831 for the latter half of the 20th century reconstructed from firn air analyses, *J. Geophys. Res. Atmos.*,
832 112(3), doi:10.1029/2006JD007208, 2007.

833 Janssens-Maenhout, G., Crippa, M., Guizzardi, D., Muntean, M., Schaaf, E., Dentener, F., Bergamaschi,
834 P., Pagliari, V., Olivier, J., Peters, J., van Aardenne, J., Monni, S., Doering, U., Petrescu, R., Solazzo, E.
835 and Oreggioni, G.: EDGAR v4.3.2 Global Atlas of the three major Greenhouse Gas Emissions for the
836 period 1970-2012, *Earth Syst. Sci. Data Discuss.*, 2010, 1–52, doi:10.5194/essd-2018-164, 2019.

837 Jiang, X., Ku, W. L., Shia, R. L., Li, Q., Elkins, J. W., Prinn, R. G. and Yung, Y. L.: Seasonal cycle of
838 N_2O : Analysis of data, *Global Biogeochem. Cycles*, 21, GB1006, doi:10.1029/2006GB002691, 2007.

839 JMA and WMO: World Meteorological Organization - Global Atmosphere Watch - World Data Centre
840 for Greenhouse Gases, Data Summary, No. 42, 101 p., [online] Available from:
841 <https://gaw.kishou.go.jp/static/publications/summary/sum42/sum42.pdf>, 2018.

842 Kaiser, J., Röckmann, T. and Brenninkmeijer, C. A. M.: Complete and accurate mass spectrometric
843 isotope analysis of tropospheric nitrous oxide, *J. Geophys. Res. Atmos.*, 108, 4476,
844 doi:10.1029/2003JD003613, D15, [2003](#).

845 [Kaiser, J., Engel, A., Borchers, R. and Röckmann, T.: Probing stratospheric transport and chemistry with](#)
846 [new balloon and aircraft observations of the meridional and vertical \$\text{N}_2\text{O}\$ isotope distribution, *Atmos.*](#)
847 [Chem. Phys., 6\(11\), 3535–3556, doi:10.5194/acp-6-3535-2006, 2006.](#)

- 848 Keller, C. A., Hill, M., Vollmer, M. K., Henne, S., Brunner, D., Reimann, S., O'Doherty, S., Arduini, J.,
849 Maione, M., Ferenczi, Z., Haszpra, L., Manning, A. J. and Peter, T.: European emissions of halogenated
850 greenhouse gases inferred from atmospheric measurements, *Environ. Sci. Technol.*, 46(1), 217–225,
851 doi:10.1021/es202453j, 2012.
- 852 Kim, K.-R. and Craig, H.: Nitrogen-15 and Oxygen-18 Characteristics of Nitrous Oxide: A Global
853 Perspective, *Science*, 262, 1855-1857, 1993.
- 854 Lebeque, B., Schmidt, M., Ramonet, M., Wastine, B., Yver Kwok, C., Laurent, O., Belviso, S., Guemri,
855 A., Philippon, C., Smith, J. and Conil, S.: Comparison of nitrous oxide (N₂O) analyzers for high-precision
856 measurements of atmospheric mole fractions, *Atmos. Meas. Tech.*, 9(3), 1221–1238, doi:10.5194/amt-9-
857 1221-2016, 2016.
- 858 Logan, J. A., Staehelin, J., Megretskaia, I. A., Cammas, J. P., Thouret, V., Claude, H., De Backer, H.,
859 Steinbacher, M., Scheel, H. E., Stbi, R., Frhlich, M. and Derwent, R.: Changes in ozone over Europe:
860 Analysis of ozone measurements from sondes, regular aircraft (MOZAIC) and alpine surface sites, *J.*
861 *Geophys. Res. Atmos.*, 117(9), 1–23, doi:10.1029/2011JD016952, 2012.
- 862 Mohn, J., Guggenheim, C., Tuzson, B., Vollmer, M. K., Toyoda, S., Yoshida, N. and Emmenegger, L.: A
863 liquid nitrogen-free preconcentration unit for measurements of ambient N₂O isotopomers by QCLAS,
864 *Atmos. Meas. Tech.*, 3(3), 609–618, doi:10.5194/amt-3-609-2010, 2010.
- 865 Mohn, J., Tuzson, B., Manninen, A., Yoshida, N., Toyoda, S., Brand, W. A. and Emmenegger, L.: Site
866 selective real-time measurements of atmospheric N₂O isotopomers by laser spectroscopy, *Atmos. Meas.*
867 *Tech.*, 5(7), 1601–1609, doi:10.5194/amt-5-1601-2012, 2012.
- 868 Mohn, J., Wolf, B., Toyoda, S., Lin, C. T., Liang, M. C., Brüggemann, N., Wissel, H., Steiker, A. E.,
869 Dyckmans, J., Szwec, L., Ostrom, N. E., Casciotti, K. L., Forbes, M., Giesemann, A., Well, R., Doucett,
870 R. R., Yarnes, C. T., Ridley, A. R., Kaiser, J. and Yoshida, N.: Interlaboratory assessment of nitrous
871 oxide isotopomer analysis by isotope ratio mass spectrometry and laser spectroscopy: Current status and
872 perspectives, *Rapid Commun. Mass Spectrom.*, 28(18), 1995–2007, doi:10.1002/rcm.6982, 2014.
- 873 Nevison, C. D., Keeling, R. F., Weiss, R. F., Popp, B. N., Jin, X., Fraser, P. J., Porter, L. W. and Hess, P.
874 G.: Southern Ocean ventilation inferred from seasonal cycles of atmospheric N₂O and O₂/N₂ at Cape
875 Grim, Tasmania, *Tellus, Ser. B Chem. Phys. Meteorol.*, 57(3), 218–229, doi:10.1111/j.1600-
876 0889.2005.00143.x, 2005.
- 877 Nevison, C. D., Dlugokencky, E., Dutton, G., Elkins, J. W., Fraser, P., Hall, B., Krummel, P. B.,
878 Langenfelds, R. L., O'Doherty, S., Prinn, R. G., Steele, L. P. and Weiss, R. F.: Exploring causes of
879 interannual variability in the seasonal cycles of tropospheric nitrous oxide, *Atmos. Chem. Phys.*, 11(8),
880 3713–3730, doi:10.5194/acp-11-3713-2011, 2011.
- 881 Ogawa, M. and Yoshida, N.: Intramolecular distribution of stable nitrogen and oxygen isotopes of nitrous
882 oxide emitted during coal combustion, *Chemosphere*, 61(6), 877–887,
883 doi:10.1016/j.chemosphere.2005.04.096, 2005.
- 884 Ostrom, N. E., Gandhi, H., Coplen, T. B., Toyoda, S., Böhlke, J. K., Brand, W. A., Casciotti, K. L.,
885 Dyckmans, J., Giesemann, A., Mohn, J., Well, R., Yu, L. and Yoshida, N.: Preliminary assessment of
886 stable nitrogen and oxygen isotopic composition of USGS51 and USGS52 nitrous oxide reference gases
887 and perspectives on calibration needs, *Rapid Commun. Mass Spectrom.*, 32(15), 1207–1214,
888 doi:10.1002/rcm.8157, 2018.
- 889 Pandey Deolal, S., Brunner, D., Steinbacher, M., Weers, U. and Staehelin, J.: Long-term in situ
890 measurements of NO_x and NO_y at Jungfraujoch 1998-2009: Time series analysis and evaluation, *Atmos.*
891 *Chem. Phys.*, 12(5), 2551–2566, doi:10.5194/acp-12-2551-2012, 2012.
- 892 Park, S., Croteau, P., Boering, K. A., Etheridge, D. M., Ferretti, D., Fraser, P. J., Kim, K.-R., Krummel, P.

- 893 B., Langenfelds, R. L., van Ommen, T. D., Steele, L. P. and Trudinger, C. M.: Trends and seasonal cycles
894 in the isotopic composition of nitrous oxide since 1940, *Nat. Geosci.*, 5(4), 261–265,
895 doi:10.1038/ngeo1421, 2012.
- 896 Pérez, T., Trumbore, S. E., Tyler, S. C., Matson, P. A., I., O.-M., Rahn, T. and Griffiths, D. W. T.:
897 Identifying the agricultural imprint on the global N₂O budget using stable isotopes, *J. Geophys. Res.*,
898 106, 9869–9878, doi:10.1179/1607845413y.0000000087, 2001.
- 899 Prather, M. J., Hsu, J., Deluca, N. M., Jackman, C. H., Oman, L. D., Douglass, A. R., Fleming, E. L.,
900 Strahan, S. E., Steenrod, S. D., Søvdé, O. A., Isaksen, I. S. A., Froidevaux, L. and Funke, B.: Measuring
901 and modeling the lifetime of nitrous oxide including its variability Michael, *J. Geophys. Res. Atmos.*,
902 120, 5693–5705, doi:10.1002/2015JD023267. Received, 2015.
- 903 Prinn, R. G., Weiss, R. F., Arduini, J., Arnold, T., Dewitt, H. L., Fraser, P. J., Ganesan, A. L., Gasore, J.,
904 Harth, C. M., Hermansen, O., Kim, J., Krummel, P. B., Li, S., Loh, Z. M., Lunder, C. R. and Maione, M.:
905 History of chemically and radiatively important atmospheric gases from the Advanced Global
906 Atmospheric Gases Experiment (AGAGE), *Earth Syst. Sci. Data*, 10, 985–1018, 2018.
- 907 Prokopiou, M., Martinerie, P., Sapart, C. J., Witrant, E., Monteil, G. A., Ishijima, K., Bernard, S., Kaiser,
908 J., Levin, I., Sowers, T., Blunier, T., Etheridge, D., Dlugokencky, E., van de Wal, R. S. W. and
909 Röckmann, T.: Constraining N₂O emissions since 1940 using firn air isotope measurements in both
910 hemispheres, *Atmos. Chem. Phys.*, 2011(June), 1–50, doi:10.5194/acp-2016-487, 2017.
- 911 Prokopiou, M., Sapart, C. J., Rosen, J., Sperlich, P., Blunier, T., Brook, E., van de Wal, R. S. W. and
912 Röckmann, T.: Changes in the Isotopic Signature of Atmospheric Nitrous Oxide and Its Global Average
913 Source During the Last Three Millennia, *J. Geophys. Res. Atmos.*, 1–17, doi:10.1029/2018JD029008,
914 2018.
- 915 Rahn, T. and Wahlen, M.: A reassessment of the global isotopic budget of atmospheric nitrous oxide,
916 *Global Biogeochem. Cycles*, 14(2), 537–543, doi:10.1029/1999GB900070, 2000.
- 917 Ravishankara, A. R., Daniel, J. S. and Portmann, R. W.: Nitrous oxide (N₂O): the dominant ozone-
918 depleting substance emitted in the 21st century., *Science*, 326(5949), 123–5,
919 doi:10.1126/science.1176985, 2009.
- 920 Reay, D. S., Davidson, E. a., Smith, K. a., Smith, P., Melillo, J. M., Dentener, F. and Crutzen, P. J.:
921 Global agriculture and nitrous oxide emissions, *Nat. Clim. Chang.*, 2(6), 410–416,
922 doi:10.1038/nclimate1458, 2012.
- 923 Reimann, S., Vollmer, M. K., Folini, D., Steinbacher, M., Hill, M., Buchmann, B., Zander, R. and
924 Mahieu, E.: Observations of long-lived anthropogenic halocarbons at the high-Alpine site of Jungfraujoch
925 (Switzerland) for assessment of trends and European sources, *Sci. Total Environ.*, 391(2–3), 224–231,
926 doi:10.1016/j.scitotenv.2007.10.022, 2008.
- 927 Rigby, M., Prinn, R. G., O’Doherty, S., Montzka, S. A., McCulloch, A., Harth, C. M., Mühle, J.,
928 Salameh, P. K., Weiss, R. F., Young, D., Simmonds, P. G., Hall, B. D., Dutton, G. S., Nance, D.,
929 Mondeel, D. J., Elkins, J. W., Krummel, P. B., Steele, L. P. and Fraser, P. J.: Re-evaluation of the
930 lifetimes of the major CFCs and CH₃CCl₃ using atmospheric trends, *Atmos. Chem. Phys.*, 13(5), 2691–
931 2702, doi:10.5194/acp-13-2691-2013, 2013.
- 932 Röckmann, T., Kaiser, J. and Brenninkmeijer, C. A. M.: The isotopic fingerprint of the pre-industrial and
933 the anthropogenic N₂O source, *Atmos. Chem. Phys.*, (3), 315–323, 2003.
- 934 Röckmann, T. and Levin, I.: High-precision determination of the changing isotopic composition of
935 atmospheric N₂O from 1990 to 2002, *J. Geophys. Res. Atmos.*, 110(21), 1–8,
936 doi:10.1029/2005JD006066, 2005.
- 937 Saikawa, E., Prinn, R. G., Dlugokencky, E., Ishijima, K., Dutton, G. S., Hall, B. D., Langenfelds, R.,

938 Tohjima, Y., Machida, T., Manizza, M., Rigby, M., O'Doherty, S., Patra, P. K., Harth, C. M., Weiss, R.
939 F., Krummel, P. B., Van Der Schoot, M., Fraser, P. J., Steele, L. P., Aoki, S., Nakazawa, T. and Elkins, J.
940 W.: Global and regional emissions estimates for N₂O, *Atmos. Chem. Phys.*, 14(9), 4617–4641,
941 doi:10.5194/acp-14-4617-2014, 2014.

942 Schibig, M. F., Steinbacher, M., Buchmann, B., Van Der Laan-Luijkx, I. T., Van Der Laan, S., Ranjan, S.
943 and Leuenberger, M. C.: Comparison of continuous in situ CO₂ observations at Jungfraujoch using two
944 different measurement techniques, *Atmos. Meas. Tech.*, 8(1), 57–68, doi:10.5194/amt-8-57-2015, 2015.

945 Schilt, A., Brook, E. J., Bauska, T. K., Bagginstos, D., Fischer, H., Joos, F., Petrenko, V. V., Schaefer,
946 H., Schmitt, J., Severinghaus, J. P., Spahni, R. and Stocker, T. F.: Isotopic constraints on marine and
947 terrestrial N₂O emissions during the last deglaciation, *Nature*, 516(7530), 234–237,
948 doi:10.1038/nature13971, 2014.

949 Sepúlveda, E., Schneider, M., Hase, F., Barthlott, S., Dubravica, D., García, O. E., Gomez-Pelaez, A.,
950 González, Y., Guerra, J.C., Gisi, M., Kohlhepp, R., Dohe, S., Blumenstock, T., Strong, K., Weaver, D.,
951 Palm, N., Sadeghi, A., Deutscher, N. M., Warneke, T., Notholt, J., Jones, N., Griffith, D. W. T., Smale,
952 D., Brailsford, G. W., Robinson, J., Meinhardt, F., Steinbacher, M., Aalto, T. and Worthy, D.:
953 Tropospheric CH₄ signals as observed by NDACC FTIR at globally distributed sites and comparison to
954 GAW surface in situ measurements, *Atmos. Meas. Tech.*, 7(7), 2337–2360, doi:10.5194/amt-7-2337-
955 2014, 2014.

956 Snider, D., Thompson, K., Wagner-Riddle, C., Spoelstra, J. and Dunfield, K.: Molecular techniques and
957 stable isotope ratios at natural abundance give complementary inferences about N₂O production pathways
958 in an agricultural soil following a rainfall event, *Soil Biol. Biochem.*, 88, 197–213,
959 doi:10.1016/j.soilbio.2015.05.021, 2015a.

960 Snider, D. M., Venkiteswaran, J. J., Schiff, S. L. and Spoelstra, J.: From the ground up: Global nitrous
961 oxide sources are constrained by stable isotope values, *PLoS One*, 10(3), 1–19,
962 doi:10.1371/journal.pone.0118954, 2015b.

963 Sowers, T., Rodebaugh, A., Yoshida, N. and Toyoda, S.: Extending records of the isotopic composition of
964 atmospheric N₂O back to 1800 A.D. from air trapped in snow at the South Pole and the Greenland Ice
965 Sheet Project II ice core, *Global Biogeochem. Cycles*, 16(4), 1–10, doi:10.1029/2002GB001911, 2002.

966 Stohl, A., Forster, C., Frank, A., Seibert, P. and Wotawa, G.: Technical note: The Lagrangian particle
967 dispersion model FLEXPART version 6.2, *Atmos. Chem. Phys.*, 5, 2461–2474,
968 doi:10.3390/atmos9020076, 2005.

969 Sturm, P., Tuzson, B., Henne, S. and Emmenegger, L.: Tracking isotopic signatures of CO₂ at the high
970 altitude site Jungfraujoch with laser spectroscopy: Analytical improvements and representative results,
971 *Atmos. Meas. Tech.*, 6(7), 1659–1671, doi:10.5194/amt-6-1659-2013, 2013.

972 Sutka, R. L., Ostrom, N. E., Ostrom, P. H., Breznak, J. a, Pitt, a J., Li, F. and Gandhi, H.: Distinguishing
973 Nitrous Oxide Production from Nitrification and Denitrification on the Basis of Isotopomer Abundances
974 Distinguishing Nitrous Oxide Production from Nitrification and Denitrification on the Basis of
975 Isotopomer Abundances, *Appl. Environ. Microbiol.*, 72(1), 638–644, doi:10.1128/AEM.72.1.638, 2006.

976 Tarasova, O. A., Senik, I. A., Sosonkin, M. G., Cui, J., Staehelin, J. and Péevot, A. S. H.: Surface ozone
977 at the Caucasian site Kislovodsk High Mountain Station and the Swiss Alpine site Jungfraujoch: Data
978 analysis and trends (1990-2006), *Atmos. Chem. Phys.*, 9(12), 4157–4175, doi:10.5194/acp-9-4157-2009,
979 2009.

980 Team, R. C.: A language and environment for statistical computing. R Foundation for statistical
981 computing, 2015; Vienna, Austria, 2016.

982 Thompson, R. L., Patra, P. K., Ishijima, K., Saikawa, E., Corazza, M., Karstens, U., Wilson, C.,

983 Bergamaschi, P., Dlugokencky, E., Sweeney, C., Prinn, R. G., Weiss, R. F., O'Doherty, S., Fraser, P. J.,
984 Steele, L. P., Krummel, P. B., Saunio, M., Chipperfield, M. and Bousquet, P.: TransCom N₂O model
985 inter-comparison-Part 1: Assessing the influence of transport and surface fluxes on tropospheric N₂O
986 variability, *Atmos. Chem. Phys.*, 14(8), 4349–4368, doi:10.5194/acp-14-4349-2014, 2014a.

987 Thompson, R. L., Ishijima, K., Saikawa, E., Corazza, M., Karstens, U., Patra, P. K., Bergamaschi, P.,
988 Chevallier, F., Dlugokencky, E., Prinn, R. G., Weiss, R. F., O'Doherty, S., Fraser, P. J., Steele, L. P.,
989 Krummel, P. B., Vermeulen, A., Tohjima, Y., Jordan, A., Haszpra, L., Steinbacher, M., Van Der Laan, S.,
990 Aalto, T., Meinhardt, F., Popa, M. E., Moncrieff, J. and Bousquet, P.: TransCom N₂O model inter-
991 comparison - Part 2: Atmospheric inversion estimates of N₂O emissions, *Atmos. Chem. Phys.*, 14(12),
992 6177–6194, doi:10.5194/acp-14-6177-2014, 2014b.

993 Thoning, K. W., Tans, P. P. and Komhyr, W. D.: Atmospheric carbon dioxide at Mauna Loa Observatory:
994 2. Analysis of the NOAA GMCC data, 1974-1985, *J. Geophys. Res.*, 94(D6), 8549–8565,
995 doi:10.1029/jd094id06p08549, 1989.

996 Tian, H., Yang, J., Xu, R., Lu, C., Canadell, J., Davidson, E. A., Jackson, R., Arneeth, A., Chang, J., Ciais,
997 P., Gerber, S., Ito, A., Joos, F., Lienert, S., Messina, P., Olin, S., Pan, S., Peng, C., Saikawa, E.,
998 Thompson, R., Vuichard, N., Winiwarter, W., Zaehle, S. and Zhang, B.: Global soil nitrous oxide
999 emissions since the preindustrial era estimated by an ensemble of terrestrial biosphere models:
1000 Magnitude, attribution, and uncertainty, *Glob. Chang. Biol.*, 25(2), 640–659, doi:10.1111/gcb.14514,
1001 2019.

1002 Toyoda, S., Yoshida, N., Urabe, T., Aoki, S., Nakazawa, T., Sugawara, S. and Honda, H.: Fractionation
1003 of N₂O isotopomers in the stratosphere, *J. Geophys. Res.*, 106(D7), 7515, doi:10.1029/2000JD900680,
1004 2001.

1005 Toyoda, S., Yamamoto, S., Arai, S., Nara, H., Yoshida, N., Kashiwakura, K. and Akiyama, K.:
1006 Isotopomeric characterization of N₂O produced, consumed, and emitted by automobiles, *rapid comm*, 22,
1007 603–612, doi:10.1002/rcm, 2008.

1008 Toyoda, S., Yano, M., Nishimura, S., Akiyama, H., Hayakawa, A., Koba, K., Sudo, S., Yagi, K., Makabe,
1009 A., Tobari, Y., Ogawa, N. O., Ohkouchi, N., Yamada, K. and Yoshida, N.: Characterization and
1010 production and consumption processes of N₂O emitted from temperate agricultural soils determined via
1011 isotopomer ratio analysis, *Global Biogeochem. Cycles*, 25(2), 1–17, doi:10.1029/2009GB003769, 2011.

1012 Toyoda, S., Kuroki, N., Yoshida, N., Ishijima, K., Tohjima, Y. and Machida, T.: Decadal time series of
1013 tropospheric abundance of N₂O isotopomers and isotopologues in the Northern Hemisphere obtained by
1014 the long-term observation at Hateruma Island, Japan, *J. Geophys. Res. Atmos.*, 118(8), 3369–3381,
1015 doi:10.1002/jgrd.50221, 2013.

1016 Toyoda, S., Yoshida, N. and Koba, K.: Isotopocule analysis of biologically produced nitrous oxide in
1017 various environments, *Mass Spectrom. Rev.*, (36), 135–160, doi:doi:10.1002/mas.21459, 2017.

1018 [Toyoda, S., Yoshida, N., Morimoto, S., Aoki, S., Nakazawa, T., Sugawara, S., Ishidoya, S., Uematsu, M.,](#)
1019 [Inai, Y., Hasebe, F., Ikeda, C., Honda, H. and Ishijima, K.: Vertical distributions of N₂O isotopocules in](#)
1020 [the equatorial stratosphere, *Atmos. Chem. Phys.*, \(18\), 833–844, 2018.](#)

1021 Tuzson, B., Henne, S., Brunner, D., Steinbacher, M., Mohn, J., Buchmann, B. and Emmenegger, L.:
1022 Continuous isotopic composition measurements of tropospheric CO₂ at Jungfraujoch (3580 m a.s.l.),
1023 Switzerland: Real-time observation of regional pollution events, *Atmos. Chem. Phys.*, 11(4), 1685–1696,
1024 doi:10.5194/acp-11-1685-2011, 2011.

1025 WMO: WMO Greenhouse Gas Bulletin., 2018.

1026 Wolf, B., Merbold, L., Decock, C., Tuzson, B., Harris, E., Six, J., Emmenegger, L. and Mohn, J.: First
1027 on-line isotopic characterization of N₂O above intensively managed grassland, *Biogeosciences*, 12(8),

- 1028 2517–2531, doi:10.5194/bg-12-2517-2015, 2015.
- 1029 Xu-Ri, Prentice, I. C., Spahni, R. and Niu, H. S.: Modelling terrestrial nitrous oxide emissions and
1030 implications for climate feedback, *New Phytol.*, 196(2), 472–488, doi:10.1111/j.1469-8137.2012.04269.x,
1031 2012.
- 1032 Yoshida, N. and Toyoda, S.: Constraining the atmospheric N₂O budget from intramolecular site
1033 preference in N₂O isotopomers, *Nature*, 405(6784), 330–4, doi:10.1038/35012558, 2000.
- 1034 Yuan, Y., Ries, L., Petermeier, H., Steinbacher, M., Gómez-Pelaéz, A. J., Leuenberger, M. C.,
1035 Schumacher, M., Trickl, T., Couret, C., Meinhardt, F. and Menzel, A.: Adaptive selection of diurnal
1036 minimum variation: A statistical strategy to obtain representative atmospheric CO₂ data and its
1037 application to European elevated mountain stations, *Atmos. Meas. Tech.*, 11(3), 1501–1514,
1038 doi:10.5194/amt-11-1501-2018, 2018.
- 1039 Yung, Y. L. and Miller, C. E.: Isotopic fractionation of stratospheric nitrous oxide, *Science*, 278(5344),
1040 1778–1780, doi:10.1126/science.278.5344.1778, 1997.
- 1041 Zellweger, C., Forrer, J., Hofer, P., Nyeki, S., Schwarzenbach, B., Weingartner, E., Ammann, M. and
1042 Baltensperger, U.: Partitioning of reactive nitrogen (NO_y) and dependence on meteorological conditions
1043 in the lower free troposphere, *Atmos. Chem. Phys.*, 3(3), 779–796, doi:10.5194/acp-3-779-2003, 2003.
- 1044 Zellweger, C., Hüglin, C., Klausen, J., Steinbacher, M., Vollmer, M. and Buchmann, B.: Inter-comparison
1045 of four different carbon monoxide measurement techniques and evaluation of the long-term carbon
1046 monoxide time series of Jungfraujoch, *Atmos. Chem. Phys.*, 9(11), 3491–3503, doi:10.5194/acp-9-3491-
1047 2009, 2009.

1050

Table 1 Trends of atmospheric $\delta^{15}\text{N}^{\text{bulk}}$, $\delta^{15}\text{N}^{\text{SP}}$ and $\delta^{18}\text{O}$ at Jungfraujoch determined using discrete measurements between April 2014 and December 2018. The trends are determined for the whole dataset, the dataset filtered for free troposphere (removing data points with significant influence from plenary boundary layer) and the second-phase dataset with bi-weekly measurements (August 2016 to December 2018).

	$\delta^{15}\text{N}^{\text{bulk}}$ (‰ a^{-1})		$\delta^{15}\text{N}^{\text{SP}}$ (‰ a^{-1})		$\delta^{18}\text{O}$ (‰ a^{-1})	
	Raw	Deseasonalized	Raw	Deseasonalized	Raw	Deseasonalized
Whole dataset	$-0.059 \pm 0.012^*$	$-0.052 \pm 0.012^*$	0.069 ± 0.029	0.065 ± 0.027	0.020 ± 0.011	0.019 ± 0.011
Free troposphere	$-0.060 \pm 0.014^*$	$-0.054 \pm 0.013^*$	0.054 ± 0.034	0.036 ± 0.030	0.024 ± 0.013	0.019 ± 0.011
First phase (Apr. 2014-Feb. 2016)	-0.036 ± 0.038	-0.041 ± 0.035	$0.449 \pm 0.100^*$	$0.314 \pm 0.082^*$	$0.238 \pm 0.029^*$	$0.207 \pm 0.026^*$
Second phase (Aug. 2016-Dec. 2018)	-0.105 ± 0.049	$-0.130 \pm 0.045^*$	0.028 ± 0.067	-0.007 ± 0.066	-0.007 ± 0.042	-0.001 ± 0.040

* Indicate significance of linear regression.

Table 2 Results of the two-box model simulations and selected literature values for comparison.

	This study		RMSE ^g	Sowers et al. (2002) ^a	Röckmann et al. (2003)^b	Ishijima et al. (2007) ^{bc}	Toyoda et al. (2013) ^{ed}	Park et al. (2012) ^{de}	Prokopiou et al. (2017) ^{ef}
Air Sample Originage	NH [†] 2014-2018	NH(FTⁿ) 2014-2018		FA [‡] , IC [‡] 1745 1785-1995	FA NA	FA [‡] 1960-2001	NH [‡] 1999-2010	SH [‡] , FA [‡] 1940-2005	FA [‡] 1940-2008
α -*	0.0154±0.004	0.0154±0.004	0.65 nmol mol ⁻¹	0.0111 to 0.0128	NA	NA	NA	NA	NA
$F_{\text{anth},2018}$ (Tg N yr ⁻¹)	8.6±0.6	8.5±0.6	NA [‡]	4.2 to 5.7	6.9	NA	5.5	6.6	5.4±1.7
$\delta^{15}\text{N}_{\text{anth}}^{\text{bulk}}$ (‰)	-8.6±4	-8.5±4	0.23	-7 to -13	-11.4	-11.6	-9.84	-15.6±1.2	-18.2±2.6
$\delta^{18}\text{O}_{\text{anth}}$ (‰)	34.8±3	34.3±3	0.22	17 to 26	31.7	NA	35.95	32.0±1.3	27.2±2.6
$\delta^{15}\text{N}_{\text{anth}}^{\text{SP}}$ (‰)	10.7±4	10.7±4	0.50	NA	11.3	NA	8.52	13.1±9.4	18.0±8.6

1055 [†] NH and SH: surface atmosphere from the Northern and Southern Hemisphere, respectively; FA: firm air; IC: ice core air; [NA: not available.](#)
ⁿFT: [Jungfraujoch dataset filtered for free troposphere \(based on NO_y:CO\).](#)
* “Value” is the dimensionless constant α describing the exponential increase in the anthropogenic flux
^g RMSE refers to root mean square error. It is in nmol mol⁻¹ for α , referring to the present day tropospheric mixing ratio for N₂O. For source isotopic values, RMSE is in the unit of ‰. [Simulations with the whole dataset and the dataset filtered for free troposphere yielded the same RMSE.](#)
^a Estimates are for 1995.
^b [Estimates are for 1998; isotopic signatures of anthropogenic sources were calculated assuming modern tropospheric values to be the same as this study.](#)
^{b,c} Estimate is for 2000, for $\delta^{18}\text{O}$ calibration is not comparable.
^d Estimate is for 2012 using the “Base” scenario.
^{d,e} Estimates are for 2005.
^{e,f} δ_{anth} values are averaged values for the period of 1940-2008.

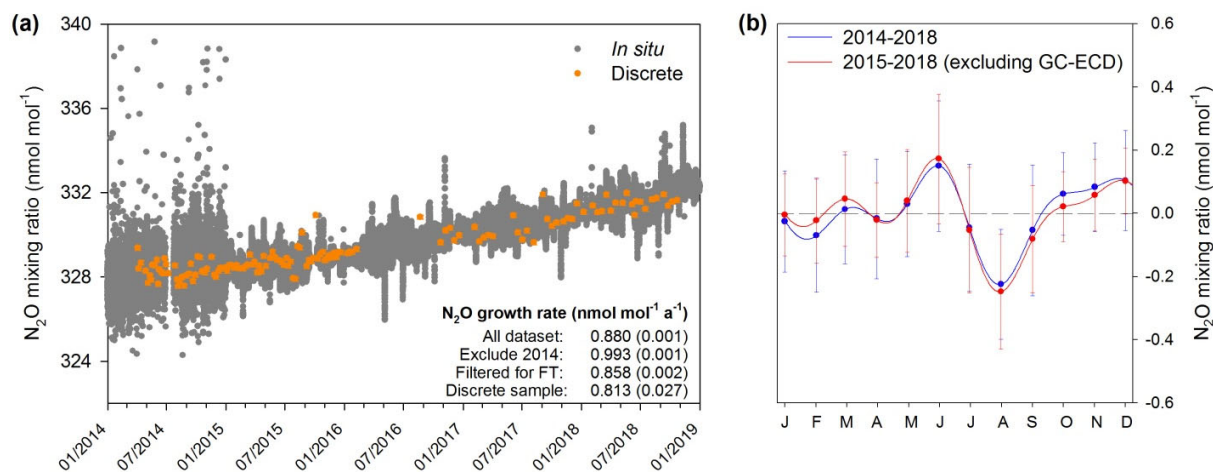
1070

Table 3 Isotopic signatures for the overall, anthropogenic and major N₂O sources contributing to N₂O variations at Jungfrauoch. Source signatures were estimated based on a “bottom-up” approach, with literature-derived isotopic signatures and fluxes for variable sources under the Swiss Meteotest emission inventory.

	Emission inventory (%)	$\delta^{15}\text{N}^{\text{bulk}}$ (‰)	$\delta^{15}\text{N}^{\text{SP}}$ (‰)	$\delta^{18}\text{O}$ (‰)	Reference
Overall source	100	-15.8 (6.2)	7.3 (3.9)	29.4 (5.5)	-
Anthropogenic source	89.4	-15.6 (6.3)	7.4 (4.0)	29.5 (5.7)	-
Agricultural emission	61.5	-17.8 (5.7)	7.2 (3.8)	29.0 (3.7)	Snider et al. (2015) Wolf et al. (2015)
Manure management	7.4	-17.5 (6.2)	6.5 (4.1)	23.9 (3.8)	Maeda et al. (2010)
Waste *	7.2	-11.5 (12.6)	10.4 (5.7)	31.3 (14.0)	Ogawa and Yoshida (2005) Snider et al. (2015)
Natural emission	10.9	-17.8 (5.7)	7.2 (3.8)	29.0 (3.7)	Snider et al. (2015) Wolf et al. (2015)

* “Waste” sources consist of both wastewater treatment and agricultural waste burning (biomass burning).

Figures



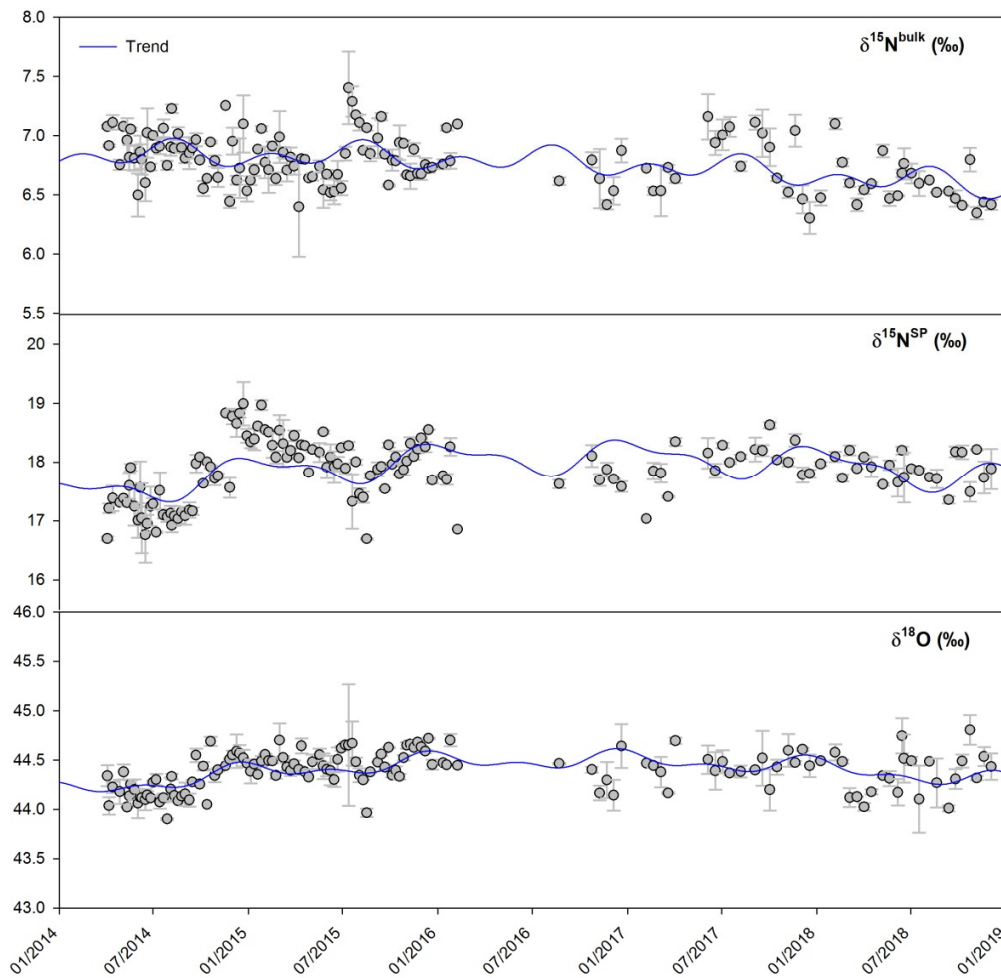
1075

1080

1085

Figure 1a *In situ* (10-min averages) and discrete measurements of N₂O mixing ratios from April 2014 to December 2018 at Jungfraujoch. *In situ* N₂O mixing ratio measurements were performed with GC-ECD method between April and December 2014. After that, OA-ICOS became the major analytical method for *in situ* measurements. Discrete sample points are presented as averages with error bars (one standard deviation). Annual N₂O growth rates determined by linear regression are given in the figure (uncertainty shown as one standard deviation). A sampling gap exists for discrete samples between February and August 2016.

1b Seasonality of N₂O mixing ratios at Jungfraujoch derived from *in situ* measurements. Datasets with/without GC-ECD measurements are compared for seasonality evaluation. The NLS model simulation for time-series gives the detrended seasonality, with error bars indicating one standard deviation of monthly residuals.



1090 **Figure 2** Time-series of isotopic composition of atmospheric N₂O observed at Jungfraujoch from April 2014 to December 2018. Error bars indicate one standard deviation of repeated measurements. Blue lines indicate the simulated trends by the NLS model.

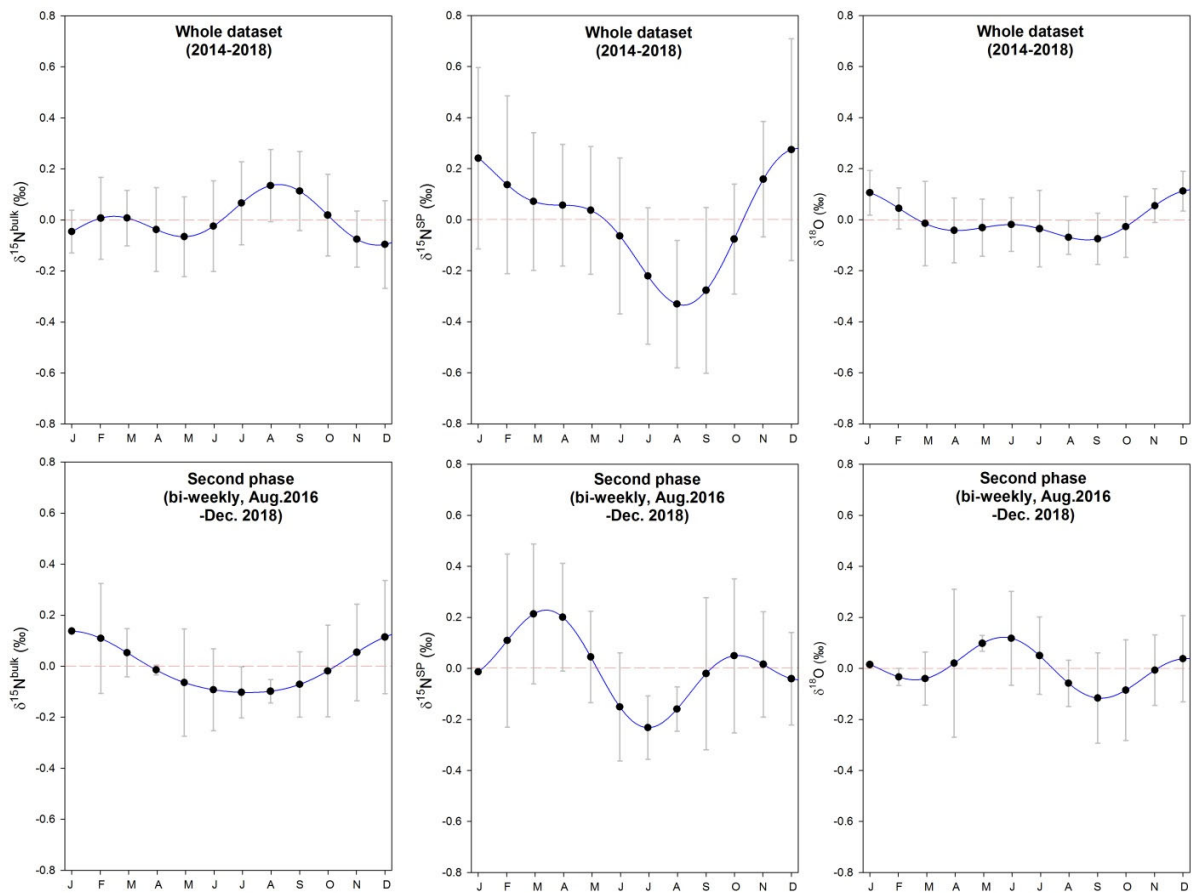
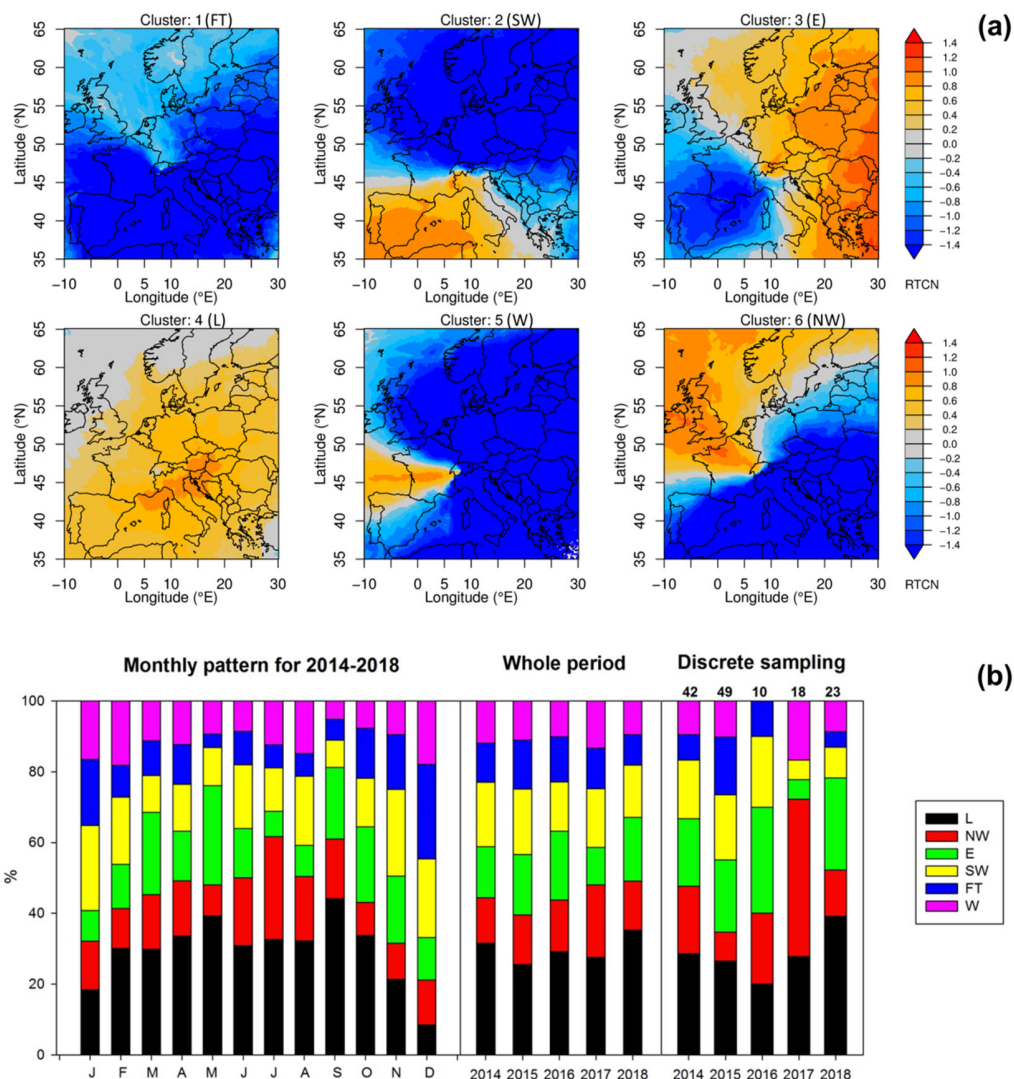


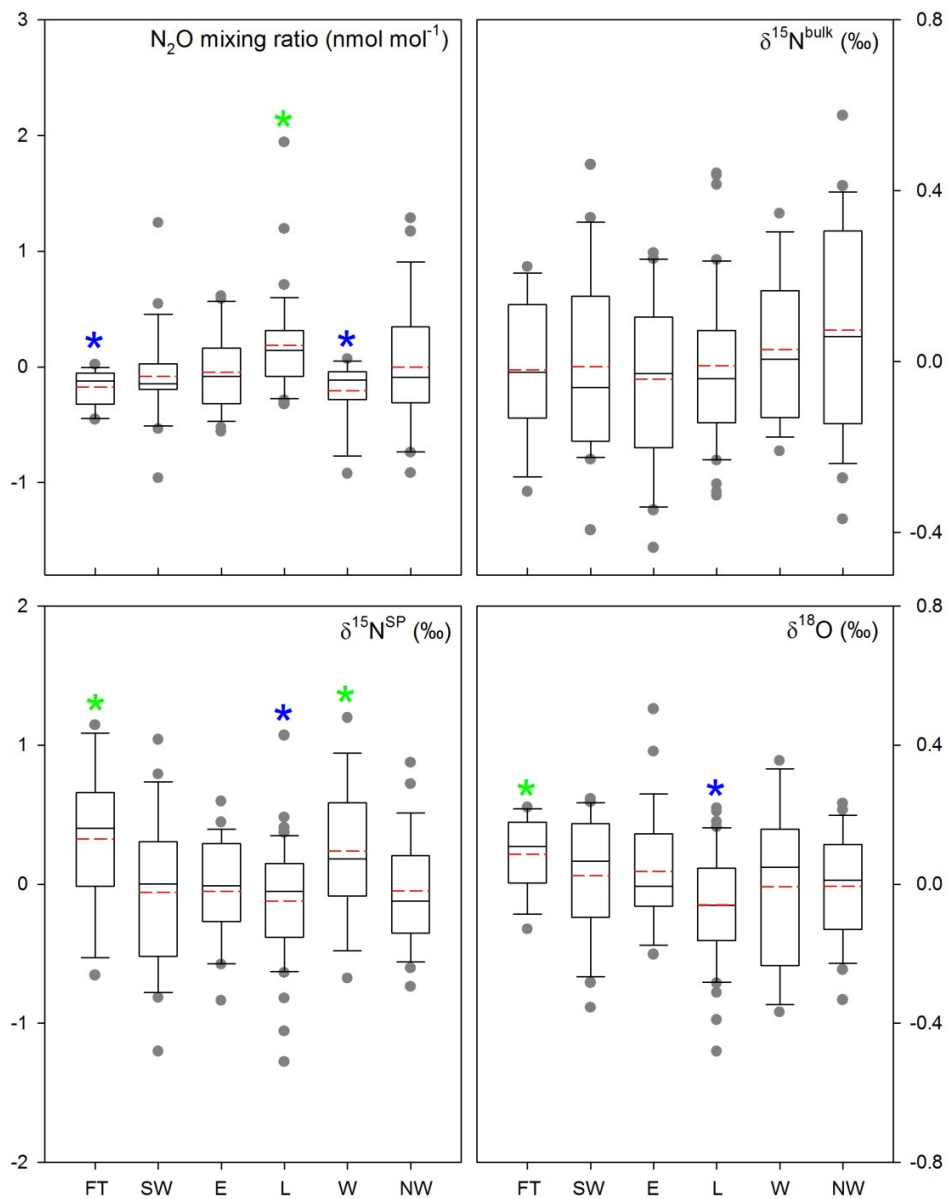
Figure 3 Seasonality of isotopic signatures of atmospheric N₂O observed at Jungfraujoch. Top panels: seasonality obtained using the whole dataset from April 2014 to December 2018; lower panels: seasonality obtained using bi-weekly data collected between August 2016 and December 2018. Red dashed lines refer to zero variability. The NLS model simulation for time-series gives the detrended seasonality, with error bars indicating one standard deviation of monthly residuals.

1095



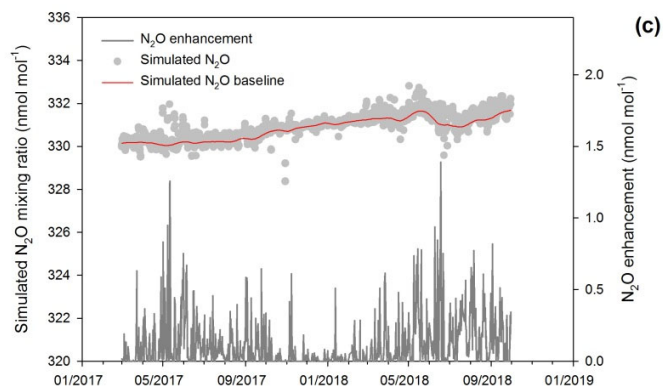
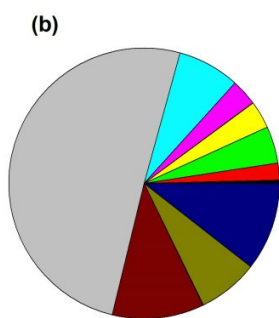
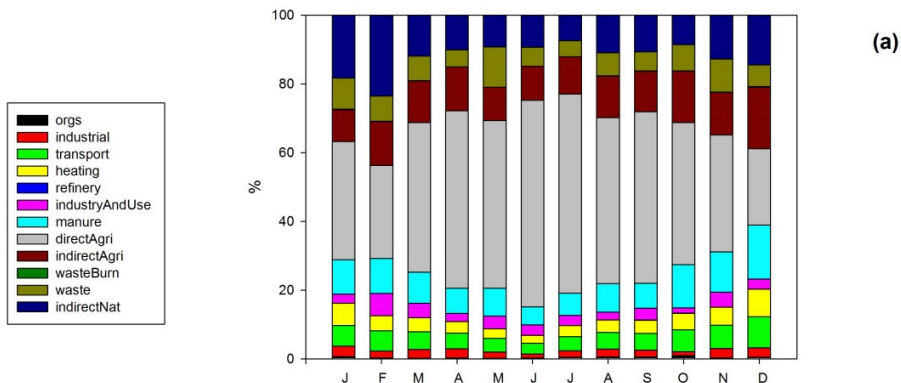
1100 **Figure 4a** Clusters of air mass transport regimes for Jungfraujoch shown as normalized surface source sensitivities over our sampling period. Cluster abbreviations refer to Free Troposphere (FT), Southwest (SW), East (E), Local (L), West (W) and Northwest (NW). The normalization was done by calculating the difference between cluster average source sensitivity and whole period average source sensitivities, divided by the period average. Orange colors indicate the main source regimes in each cluster, whereas blue colors indicate little to no influence on Jungfraujoch observations. The free tropospheric cluster showed lower than average surface sensitivity everywhere.

1105 **4b** Cluster frequency of air mass transport regimes (%) shown as a monthly pattern (left) and interannual patterns for the whole periods (middle) and for the periods of discrete sampling (right). Numbers above the right figure indicate the total number of discrete samples per year.



1110

Figure 5 Comparison of N₂O mixing ratios and isotopic signatures (with linear trends removed) for the six air mass footprint clusters used in the present study. Green and blue stars indicate significantly larger and smaller values than the others, respectively; red dashed lines indicate mean levels; grey points indicate outliers.



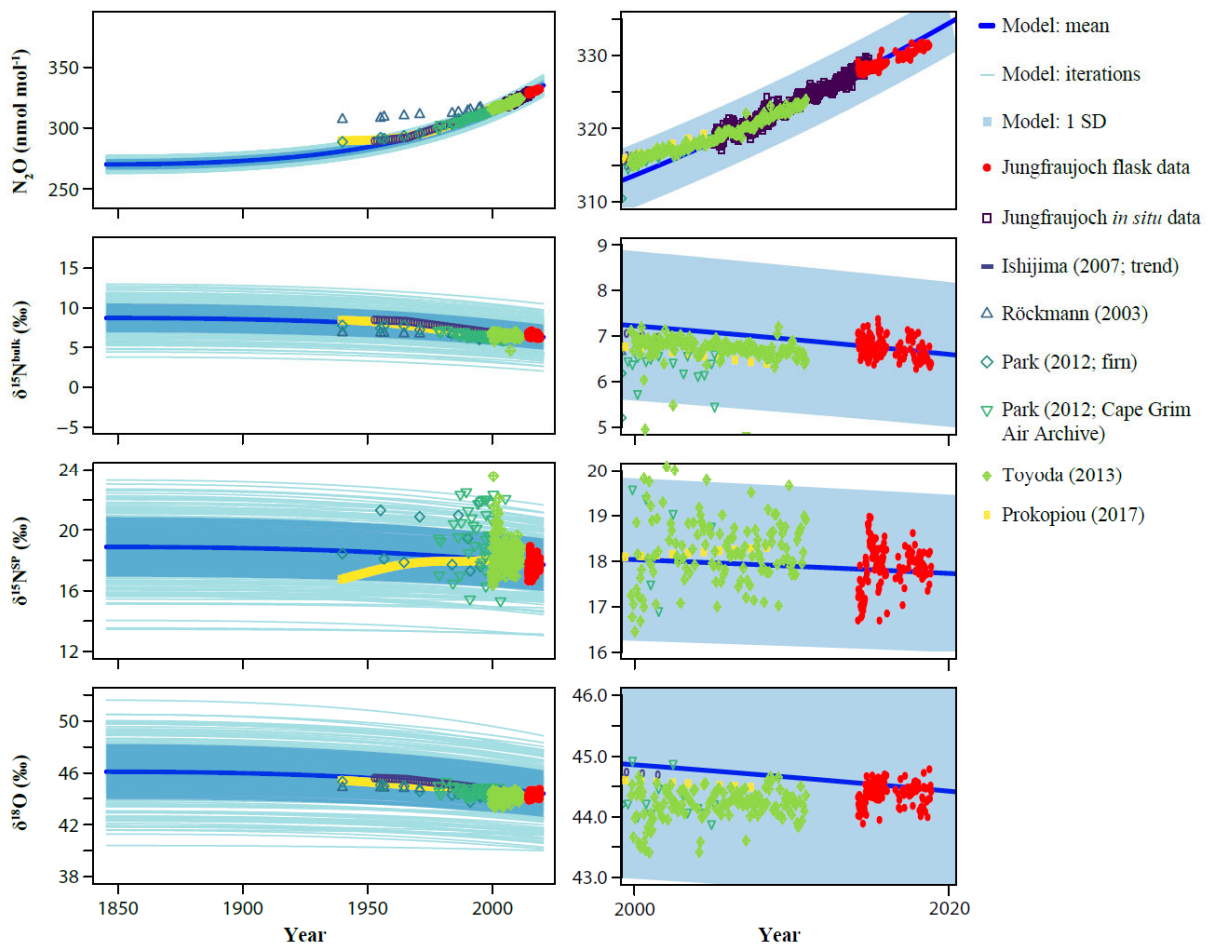
1115

Figure 5a-6a Mean monthly stacked-bar plots of source contributions (%) to atmospheric N₂O at Jungfrauoch derived from inversion modeling.

5b-6b Overall contributions of N₂O sources responsible for emission to Jungfrauoch.

1120

5e-6c Simulated 3-hourly N₂O mixing ratios, N₂O mixing ratio baseline and N₂O enhancements in nmol mol⁻¹.



1125 | **Figure 6-7** Two-box model results showing the influence of anthropogenic emissions on N_2O mixing ratio and isotopic composition in the troposphere. Left: full time range from the start of the anthropogenic period (1845) to present day; Right: zoom to the last two decades. Isotopic measurements at Jungfraujoch were used as the only constraint of current tropospheric N_2O isotopic composition for the model. See the materials and method as well as the SI for more details and other input parameters. Atmospheric as well as firn air measurements of $\delta^{15}\text{N}^{\text{bulk}}$, $\delta^{15}\text{N}^{\text{SP}}$ and $\delta^{18}\text{O}$ from the literature are presented for comparison. Blue shaded areas indicate one standard deviation of the model iterations.